Am J Cancer Res 2025;15(3):894-928
www.ajcr.us /ISSN:2156-6976/ajcr0163163

Original Article

Epigenetic regulation and tumor suppressive function of lncRNA EP300-AS1 in nasopharyngeal carcinoma through activation of TFAP2C binding to CST6: implications for diagnosis, prognosis, and therapy

Chengliang Xing[1*], Shun Ding[1*], Tingting Duan[1*], Zhiqun Li[1], Jinren Yan[1], Yu Kuang[2], Qibing Liu[3], Zhonglin Mu[1]

[1]Department of Otolaryngology, Head and Neck Surgery, The First Affiliated Hospital of Hainan Medical University, Haikou 570102, Hainan, China; [2]Medical Physics Program, University of Nevada, Las Vegas, Las Vegas, NV 89154, USA; [3]Department of Pharmacy, The First Affiliated Hospital of Hainan Medical University, Haikou 570102, Hainan, China. [*]Equal contributors and co-first authors.

Received January 7, 2025; Accepted February 5, 2025; Epub March 15, 2025; Published March 30, 2025

Abstract: The long non-coding RNA EP300-AS1 (lncRNA EP300-AS1), identified as a potential regulatory factor in various cancers, remains underexplored in nasopharyngeal carcinoma (NPC). This study investigated EP300-AS1's regulatory mechanisms in NPC, particularly its interaction with transcription factor AP-2 Gamma (TFAP2C) and its effect on cystatin E/M (CST6) expression. Employing clinical samples and NPC cell lines, we conducted in vitro and in vivo xenograft experiments to assess the impacts of modulating EP300-AS1 expression. Techniques such as CCK8, migration, scratch, apoptosis assays, cell cycle analysis, immunoblotting, and fluorescence experiments elucidated EP300-AS1's role in NPC. The interaction between EP300-AS1 and TFAP2C in regulating CST6 expression was verified using FISH, ChIP, RNA pull-down, and silver staining assays. Results indicated lower expression levels of EP300-AS1 and CST6 in NPC, with EP300-AS1 suppression inhibiting cell proliferation, migration, and invasion, while promoting apoptosis and maintaining the cell cycle in the G1 phase. EP300-AS1 also modulated epithelial-mesenchymal transition (EMT) marker expression, suggesting a role in metastasis control. Conclusively, EP300-AS1 acts as a potential tumor suppressor in NPC by interacting with TFAP2C and targeting CST6, offering novel biomarkers and therapeutic targets through its influence on methylation and the tumor microenvironment.

Keywords: lncRNA EP300-AS1, CST6, nasopharyngeal carcinoma, prognosis

Introduction

NPC, a subtype of head and neck squamous carcinoma (HNSC), originates from the nasopharyngeal epithelial cells [1, 2]. It is especially common in certain geographical regions, such as southern China and parts of Southeast Asia, with annual incidence rates reaching up to 30 cases per 100,000 individuals [3]. Although significant progress has been made in radiation therapy techniques with imaging guidance, which is the primary treatment approach for NPC, the complex anatomical location of the nasopharynx often leads to local recurrences and distant metastases in approximately 20% and 30% of patients, respectively [4]. As a result, the 5-year survival rate remains low, particularly for patients with advanced stages, due to such recurrence and metastases [5]. This highlights the urgent need to identify novel and effective treatment strategies for NPC, aiming to improve patient prognosis.

The molecular mechanisms underlying the development and progression of NPC are not yet fully elucidated. Recent progress in molecular biology has revealed the important roles of long non-coding RNAs (lncRNAs) in various cancer types, including NPC. Among these, the lncRNA EP300-AS1 has emerged as a potential key player in the pathogenesis of NPC.

lncRNAs are molecules longer than 200 nucleotides that do not code for proteins [6]. They play

https://doi.org/10.62347/MCYV5235

essential roles in regulating gene expression and cellular processes and are increasingly recognized for their involvement in various human diseases, including cancer. lncRNAs contribute to embryonic development, cell proliferation, tissue differentiation [7], and processes such as tumor growth, apoptosis, invasion, and metastasis [8, 9]. Among these, EP300-AS1 (RP1-85F18.6), located on human chromosome 22, acts as an antisense transcript of the EP300 gene [10]. This lncRNA has attracted interest for its potential regulatory functions in multiple cancer types [11, 12]. Studies suggest that low expression of EP300-AS1 is linked to cancer occurrence and progression. In cervical cancer, reduced EP300-AS1 expression correlates with poor patient prognosis, implying its role in tumor suppression. EP300-AS1 can exhibit suppressive effects within specific microenvironments by modulating oncogene expression, highlighting its dual role in tumorigenesis [13]. However, the expression and function of lncRNA EP300-AS1 in nasopharyngeal carcinoma (NPC) remain unclear and warrant further investigation.

Cystatin E/M (CST6), a member of the type 2 cystatin family, consists of extracellular polypeptide inhibitors of cysteine proteases that prevent further protein degradation [14]. CST6 is a 149-amino acid protein with a 28-residue signal peptide and inhibits key proteases such as cathepsin B (CTSB), cathepsin L (CTSL), and legumain (LGMN). Widespread epigenetic silencing of CST6 has been reported in various cancer types [15-17].

Our previous bioinformatic analysis revealed the downregulation of CST6 in HPV-positive HNSC samples [18]. Interestingly, the dynamic expression change of CST6 seemed to correspond with its dual function in different cancer types. We further found that DNA methylation in the CST6 promoter region globally regulated its gene expression. The downregulation of CST6 in HPV-positive HNSC samples suggests a dynamic expression pattern, potentially associated with its dual function in different cancer types. CST6 expression was positively correlated with epithelial cell infiltration, which is involved in EMT and cell proliferation [18]. However, the therapeutic potential of CST6 in NPC and its role in regulating metastasis remain to be explored.

This study aims to investigate the role of lncRNA EP300-AS1 in the progression and development of NPC. We examined its interaction with the transcription factor AP-2 Gamma (TFAP2C), a known regulator in cancer biology, to understand its combined impact on NPC. Furthermore, we explored the influence of lncRNA EP300-AS1 on the expression of CST6, which is associated with tumor suppression and cellular stability. This research employs a comprehensive approach, utilizing clinical nasopharyngeal tissues and NPC cell lines, along with various molecular biology techniques. Through both in vitro and in vivo studies, we aim to elucidate the functional dynamics of EP300-AS1 and its interactions with TFAP2C and CST6. By deepening our understanding of these molecular interactions, we hope to contribute to the growing knowledge of NPC and provide new insights for targeted therapeutic strategies.

Materials and methods

Study design

Gene expression analysis: We designed the study to investigate the role of lncRNA EP300-AS1 in NPC using a multi-faceted approach. Initially, we performed a comprehensive gene expression analysis using The Cancer Genome Atlas (TCGA) and Gene Expression Omnibus (GEO) datasets.

Diagnostic and prognostic analysis: We employed Receiver Operating Characteristic (ROC), survival analysis, and functional enrichment analysis to evaluate the potential of lncRNA EP300-AS1 as a diagnostic biomarker, as well as its prognostic significance in HNSCC.

In vitro cell line experiments: To further explore the functional role of lncRNA EP300-AS1, we conducted a series of in vitro cell line experiments. These experiments involved modulating EP300-AS1 expression in NPC cell lines and assessing the effects on cell proliferation, migration, and clonogenic potential using various assays such as CCK-8, wound healing, and colony formation assays.

Epigenetic mechanism exploration: We also delved into the epigenetic regulation mechanisms of lncRNA EP300-AS1 and its downstream targets. Methylation-specific PCR and

chromatin immunoprecipitation (ChIP) assays were employed to investigate how methylation influences EP300-AS1 expression and its interaction with key proteins.

NPC xenograft models in BALB/c nude mice: To validate the in vitro findings and observe the effects of EP300-AS1 modulation in a living organism, we established NPC xenograft models in BALB/c nude mice. This in vivo component of the study was crucial in assessing the translational relevance of the findings and the potential therapeutic implications of targeting EP300-AS1 in NPC.

Clinical sample acquisition

This study collected biopsy samples from 10 patients diagnosed with nasopharyngeal carcinoma (NPC) and 10 normal nasopharyngeal tissue samples (used as negative controls), all sourced from the First Affiliated Hospital of Hainan Medical University. The inclusion criteria for the NPC group were: 1) a confirmed diagnosis of nasopharyngeal carcinoma; 2) age between 18 and 75 years; 3) no other head and neck tumors or systemic diseases; and 4) no prior chemotherapy or radiation therapy. Exclusion criteria included: 1) a history of other malignant tumors; 2) severe infections, immune system diseases, or other systemic conditions; and 3) prior treatment for nasopharyngeal carcinoma (e.g., chemotherapy or radiation therapy) before sample collection.

The inclusion criteria for the control group were: 1) normal nasopharyngeal tissue confirmed by clinical presentation and pathological examination; 2) matched age and sex with the NPC patient group; and 3) no history of nasopharyngeal-related diseases or significant systemic conditions. Exclusion criteria for the control group included: 1) a history of nasopharyngeal disease or head and neck tumors; and 2) immune system diseases, severe infections, or other systemic conditions that could affect nasopharyngeal tissue. Written approval for the study was obtained from the hospital's Institutional Ethics Review Board, and all participants signed informed consent forms before sample collection.

Sample Collection and Ethics Statement: NPC specimens were obtained from patients undergoing surgical procedures at the First Affiliated Hospital of Hainan Medical University. All patients provided informed consent for the use of their tissue in research, and the study protocol was approved by the Institutional Review Board of the hospital (Number: No. 1, 2022). All experiments and procedures were performed by the ethical standards laid down in the 1964 Declaration of Helsinki and its later amendments.

Data collection from public databases

The lncRNA EP300-AS1 has been suggested to serve as a potential biomarker for cancer diagnosis and may have important roles in various cancer types [19, 20]. However, previous studies investigating EP300-AS1's expression in cancer have been restricted to small sample sizes and specific cancer types. To address this limitation, we comprehensively analyzed the expression pattern of lncRNA EP300-AS1.

mRNA sequencing data along with clinicopathological details of all patients were acquired from TCGA and GEO databases. From the TCGA database, we downloaded and organized RNA-seq data processed via the STAR pipeline from 33 cancer projects, extracting expression data in TPM format.

To meet statistical requirements, the expression data for EP300-AS1 was processed using a log2(value + 1) transformation. We analyzed HNSC tumor tissues and normal tissues using paired and unpaired analyses. To identify genes whose expression patterns significantly correlate with EP300-AS1, we further conducted gene association studies and identified the top 100 most significantly associated genes using R package 'stat'. The analysis was conducted using R software (version 4.2.1). Statistical analysis was performed using the Wilcoxon rank-sum test, and the results were visualized with the ggplot2 package.

For the GEO database, we downloaded the data (GSE12452 and GSE64634) in MINiML format, which encompasses complete information for all platforms, samples, and GSE records within those datasets. For datasets that were not normalized, we applied a uniform log2 transformation. For those datasets that lacked standardization, we utilized the 'normalize.quantiles' function from the R package 'preprocessCore' to standardize the data. Probes corresponding

Table 1. Reverse transcription-quantitative polymerase chain reaction primers utilized in this study

Gene name	Primer sequence (5'-3')
lncRNA EP300-AS1	Forward: GGCTCTTTGCTCACATCG
	Reverse: AAGGAAACCACAGGCTCA
CST6	Forward: TGGTCGGAGAACTCCGGGACCTG
	Reverse: CACAGCGCAGCTTCTCCTGCTGC
β-actin	Forward: CCAGCCTTCCTTCTTGGGTA
	Reverse: TCTTTACGGATGTCAACGTCAC

to multiple genes were removed, and the average value of multiple probes for the same gene was calculated. In cases where different batches existed within the same dataset and platform, we employed the 'removeBatchEffect' function from the R package 'limma' to eliminate batch effects. Various analyses, including survival analysis, differential expression analysis, gene identification, and investigation of immune infiltrates, were conducted using survival analysis tools (GEPIA, MethSurv, and TIMER). To gain insights into the functional role of lncRNA EP300-AS1, we performed functional enrichment analysis using the R package (clusterProfiler).

Cell line establishment and culture

Our study utilized the CNE1 and 5-8F cell lines, which are widely used and representative in NPC research studies [21, 22]. As a control, the human immortalized nasopharyngeal epithelial cell line NP69 was used. The nasopharyngeal cancer cell lines CNE1 and 5-8F were obtained from Ningbo Mingzhou Biotechnology Co., while immortalized human nasopharyngeal epithelial cells NP69 were procured from Qingqi Biotechnology Development Co. These cell lines were cultured in RPMI-1640 medium supplemented with 10% fetal bovine serum and 1% penicillin-streptomycin for CNE1 and 5-8F cells, and in DMEM media supplemented similarly for NP69 cells. Cultures were maintained at 37°C in a humidified atmosphere with 5% CO_2.

RT-qPCR analysis

RNA extraction and cDNA synthesis: Total RNA was extracted from cultured cells using TRIzol reagent, following the manufacturer's protocol. The integrity and concentration of RNA were assessed using a NanoDrop spectrophotometer. To eliminate genomic DNA contamination, RNA samples underwent DNase I treatment. Subsequently, 1 μg of RNA was reverse transcribed into cDNA using the Takara PrimeScript RT Reagent Kit, with reaction conditions as provided by the manufacturer.

Real-time quantitative PCR (RT-qPCR): The synthesized cDNA was amplified using FastFire qPCR PreMix containing SYBR Green I dye. Each qPCR reaction was set up in a total volume of 20 μL and run in a 7500 Fast Real-Time PCR System. Thermal cycling conditions included initial denaturation at 95°C for 2 minutes, followed by 40 cycles of 95°C for 10 seconds and 60°C for 30 seconds. Melting curve analysis was performed for specificity verification.

Internal control and data analysis: β-actin served as an internal control to normalize the expression levels of target genes. Primers for β-actin and target genes were designed using Primer-BLAST and synthesized commercially (**Table 1**). Relative expression levels of genes were calculated using the $2^{-\Delta\Delta Ct}$ method, normalizing target gene expression against β-actin and comparing it to a control sample. Data were presented as mean ± standard deviation (SD) from three independent experiments.

Histology

Tissue Collection and Fixation: Tissue samples were collected following standard surgical or biopsy procedures. Immediately after collection, the samples were immersed in 10% neutral buffered formalin for fixation. The fixation process was carried out at room temperature for 24 hours to preserve the tissue architecture and cellular details. This step is critical for preventing autolysis and decomposition of the tissues.

Dehydration and Clearing: Post fixation, the tissue samples underwent a series of dehydration steps. The samples were first washed in phosphate-buffered saline (PBS) to remove excess formalin and then dehydrated through a graded series of alcohol washes. This involved sequential immersion in 70%, 80%, 90%, and 100% isopropanol, each for 1 hour, to remove water from the tissues. Following dehydration, the tissues were cleared in xylene for 2 hours. Xylene

helps in removing alcohol and preparing the tissue for infiltration with paraffin.

Paraffin Embedding: After clearing, the tissues were infiltrated with paraffin wax. The samples were placed in a tissue cassette and immersed in molten paraffin at 60°C for at least 4 hours, allowing the paraffin to penetrate thoroughly. The infiltrated tissues were then embedded in blocks of paraffin wax in a mold. These blocks were cooled at room temperature to solidify, creating a firm matrix that supports the tissue for sectioning.

Sectioning and Staining: The paraffin-embedded tissue blocks were sectioned at a thickness of 4-5 micrometers using a microtome. The thin sections were carefully mounted on glass slides and dried overnight at 37°C to enhance adhesion to the glass. For histological examination, the sections were deparaffinized in xylene and rehydrated through a graded series of alcohol (100%, 90%, 80%, and 70%) followed by water. Hematoxylin and Eosin (H&E) staining was performed for histological examination. Hematoxylin stains the cell nuclei blue, highlighting details such as chromatin and nucleoli, while eosin stains the cytoplasm and extracellular matrix in varying shades of pink. The slides were then dehydrated, cleared, and mounted with a coverslip using a mounting medium.

Microscopic Examination and Analysis: The stained tissue sections were examined under a light microscope by a qualified pathologist. The evaluation included the assessment of tissue architecture, cellular morphology, and the identification of any pathological changes. Photomicrographs were taken as needed for documentation and further analysis.

Immunohistochemistry

Tissue Preparation and Antigen Retrieval: The NPC specimens were fixed in 10% neutral buffered formalin immediately after excision and embedded in paraffin. Sections of 4 μm thickness were cut and mounted on positively charged slides. For antigen retrieval, the sections were deparaffinized in xylene and rehydrated through a graded series of ethanol. Antigen retrieval was performed by heating the slides in a citrate buffer (pH 6.0) at 95°C for 20 minutes in a water bath. This step was crucial for unmasking antigen epitopes and enhancing antibody binding.

Immunostaining: After antigen retrieval, endogenous peroxidase activity was blocked by treating the sections with 3% hydrogen peroxide for 10 minutes at room temperature. Non-specific binding was minimized by incubating the sections with blocking serum for 30 minutes. The sections were then incubated with the primary antibody anti-CST6 (dilution 1:200; ABCAM, Cambridge, UK) at 4°C overnight in a humidified chamber. Following primary antibody incubation, the sections were washed with PBS and then incubated with a biotinylated secondary antibody for 30 minutes at room temperature.

Visualization and Counterstaining: The immunoreactivity was visualized using the DAB (3,3'-Diaminobenzidine) chromogen substrate kit, resulting in a brown-colored precipitate at the antigen site. After the DAB reaction, the sections were counterstained with Harris hematoxylin for 1 minute to stain the nuclei.

Image Analysis: The stained slides were examined under a light microscope, and representative areas were photographed. The immunoreactivity of CST6 was quantified by measuring the Integrated Optical Density (IOD) and area of staining in the digital images. Image analysis was performed using Image J software version 6.0. The ratio of IOD to the area (IOD/Area ratio) was calculated to provide a quantitative measure of CST6 expression in the tissues. This ratio was used for comparative analysis across different samples.

Immunofluorescent analysis

Sample Preparation and Permeabilization: For immunofluorescent staining, cells were grown on coverslips to an appropriate confluency. After reaching the desired confluence, cells were washed with phosphate-buffered saline (PBS) and fixed with 4% paraformaldehyde for 15 minutes at room temperature to preserve cellular structures. Following fixation, cells were permeabilized with 0.1% Triton X-100 in PBS for 10 minutes to allow entry of antibodies into the cells.

Blocking Non-specific Binding: To block non-specific binding sites, the cells were incubated in a blocking buffer, typically 5% bovine serum

albumin (BSA) in PBS, for 1 hour at room temperature. This step is crucial to reduce background staining and enhance the specificity of antibody binding.

Antibody Incubation: After blocking, the cells were incubated with primary antibodies against CST6, E-cadherin, and N-cadherin, each diluted to 1:300 in blocking buffer. The incubation with primary antibodies was performed overnight at 4°C in a humidified chamber. This step allows for the specific binding of the antibodies to their respective antigens in the cells.

Secondary Antibody Incubation: Following primary antibody incubation, the cells were washed with PBS to remove unbound primary antibodies and then incubated with fluorescently labeled secondary antibodies, diluted to 1:500 in blocking buffer. The incubation with secondary antibodies was done for 1 hour at room temperature in the dark. The choice of secondary antibodies depended on the species of the primary antibodies and was conjugated with fluorophores suitable for fluorescence microscopy.

Nuclear Staining: After secondary antibody incubation, cells were washed and stained with 4',6-diamidino-2-phenylindole (DAPI) for 5 minutes to visualize the nuclei. DAPI binds strongly to A-T rich regions in DNA, providing a blue fluorescence signal upon binding.

Mounting and Imaging: Post staining, the coverslips were washed and mounted onto glass slides using an anti-fade mounting medium to preserve the fluorescence. The slides were then examined under a fluorescence microscope. Images were captured using appropriate filters for the fluorophores used. Care was taken to adjust the exposure settings to prevent signal saturation and to ensure that the fluorescence signals were within the dynamic range of the imaging system.

Image Analysis: The acquired images were analyzed using image analysis software. The fluorescence intensity of CST6, E-cadherin, and N-cadherin staining was quantified, and the localization of these proteins within the cells was examined. Additionally, the nuclear staining with DAPI was used to assess the number and morphology of the cells.

Plasmid transfection

Cell Culture and Preparation: Cells suitable for the study were cultured in appropriate growth medium under standard conditions (37°C, 5% CO_2). Prior to transfection, cells were seeded in 6-well plates and allowed to reach 70-80% confluence. This confluency level is critical to ensure efficient transfection while maintaining cell viability.

Transfection Reagents and Plasmids: Plasmid DNA constructs used for the transfection included pEGFP-C1 (control vector), pEGFP-C1-lncRNA EP300-AS1, and pEGFP-C1-CST6. These plasmids were prepared using a high-quality plasmid DNA purification kit to achieve optimal transfection efficiency. Lipofectamine 3000 (Invitrogen, Carlsbad, CA, USA), a widely used transfection reagent, was chosen for its high efficiency and low cytotoxicity.

Transfection Procedure: For transfection, Lipofectamine 3000 was diluted in Opti-MEM Reduced Serum Medium (Gibco, Life Technologies) and mixed with the respective plasmid DNA according to the manufacturer's protocol. The DNA-Lipofectamine 3000 complexes were allowed to form for 15 minutes at room temperature. Subsequently, the complexes were added dropwise to the cells in the 6-well plates. Cells were incubated with the transfection mixture for 6 hours, after which the medium was replaced with fresh growth medium to reduce cytotoxicity.

Post-transfection Incubation: Following transfection, cells were incubated for 48 hours to allow sufficient time for gene expression. This period is crucial for the expression of the transfected genes and the subsequent GFP (Green Fluorescent Protein) tagging, which facilitates the visualization and confirmation of successful transfection.

Validation of Transfection: RT-qPCR Analysis: To validate the overexpression or knockdown of lncRNA EP300-AS1 and CST6, RT-qPCR was performed 48 hours post-transfection. Total RNA was extracted from the transfected cells, and cDNA was synthesized. qPCR was conducted using specific primers for EP300-AS1, CST6, and a housekeeping gene (e.g., GAPDH) for normalization. The relative expression levels were

calculated to assess the efficiency of transfection.

Western Blot Analysis: In parallel, Western blot analysis was conducted to validate the protein expression. Cells were lysed, and protein concentrations were determined. Equal amounts of protein were separated by SDS-PAGE, transferred to a PVDF membrane, and probed with primary antibodies specific to the target proteins and a secondary antibody conjugated with a detection enzyme. The protein bands were visualized using an appropriate detection system, and the intensity of the bands was quantified to confirm the expression of the target proteins.

Stable cell line construction

Cell Line Selection and Culture: The CNE1 and 5-8F cell lines were chosen for stable transfection due to their relevance in NPC research. Cells were cultured in RPMI-1640 medium (Gibco, Life Technologies) supplemented with 10% fetal bovine serum (FBS) and 1% penicillin-streptomycin, and maintained at 37°C in a humidified atmosphere containing 5% CO_2.

Plasmid Constructs for Stable Transfection: Plasmid vectors containing the sequences for lncRNA EP300-AS1 and CST6, along with a neomycin resistance gene for selection, were prepared. The integrity and concentration of the plasmid DNA were verified through agarose gel electrophoresis and spectrophotometric analysis, respectively.

Transfection Procedure: For transfection, CNE1 and 5-8F cells were seeded in 6-well plates and allowed to reach 70-80% confluence. The transfection of cells with the respective plasmids was performed using Lipofectamine 3000 reagent, following the manufacturer's instructions. Briefly, the plasmid DNA was mixed with Lipofectamine in Opti-MEM Reduced Serum Medium and incubated to form complexes, which were then added to the cells. The cells were incubated with the DNA-Lipofectamine complexes for 6 hours, after which the medium was replaced with fresh growth medium.

Selection of Stable Transfectants: Following transfection, cells were allowed to recover for 24-48 hours. The medium was then replaced with a selection medium containing neomycin (G418) at a concentration determined by a kill curve. The concentration of G418 was typically in the range of 400-800 μg/mL. The cells were cultured in this selection medium for several weeks, with regular medium changes every 2-3 days. During this period, cells that did not integrate the plasmid were eliminated, allowing for the isolation of stable transfectants.

Isolation of Stable Clones: Individual neomycin-resistant colonies were isolated using cloning cylinders or by limited dilution cloning. Clones were expanded and continuously cultured in the presence of neomycin to maintain selection pressure.

Confirmation of Overexpression: RT-qPCR Analysis: To confirm the overexpression of lncRNA EP300-AS1 and CST6 in the stable cell lines, RT-qPCR was performed. Total RNA was extracted from the stable cell lines and reverse transcribed into cDNA. qPCR was conducted using specific primers for EP300-AS1, CST6, and an internal control gene. The relative expression levels were calculated and compared to control cells (untransfected or transfected with empty vector) to confirm successful overexpression.

Verification of Stable Integration: In some cases, additional verification methods such as Southern blot or PCR can be employed to confirm the stable integration of the transgene into the host cell genome.

Maintenance and Storage: Stable cell lines were maintained under continuous neomycin selection to ensure the persistence of the transgene. Cells were regularly passaged and checked for mycoplasma contamination. For long-term storage, cells were cryopreserved in liquid nitrogen.

Cell Counting Kit-8 assay

Cell Seeding and Culture: Cells were seeded in 96-well plates at an appropriate density (typically 2,000-10,000 cells per well, depending on the cell type and growth rate) in a total volume of 100 μL of culture medium. The cells were incubated overnight at 37°C in a 5% CO_2 atmosphere to allow for attachment and recovery.

Preparation of CCK-8 Solution: The Cell Counting Kit-8 solution was prepared according to the manufacturer's instructions. The CCK-8

reagent contains a WST-8 [2-(2-methoxy-4-nitrophenyl)-3-(4-nitrophenyl)-5-(2,4-disulfophenyl)-2H-tetrazolium, monosodium salt] which produces a water-soluble formazan dye upon reduction in the presence of an electron carrier. This reagent is sensitive to light, so it was protected from direct sunlight and stored at 4°C until use.

Assay Procedure: After 24 hours of cell seeding, 10 μL of CCK-8 solution was added to each well. It is crucial to gently mix the CCK-8 solution with the culture medium by pipetting or shaking the plate to ensure uniform distribution. The cells were then incubated with the CCK-8 solution for 1-4 hours at 37°C. The duration of incubation can vary depending on the cell type and experimental conditions, and it is essential to determine the optimal incubation time in preliminary experiments.

Measurement of Absorbance: Following incubation, the absorbance of the formazan product, which correlates with the number of viable cells, was measured at 450 nm using a microplate reader. It is important to include wells with culture medium alone as a blank control. These blank readings were subtracted from the experimental readings to correct for background absorbance.

Data Analysis: The absorbance values reflect the cell viability and proliferation. The results were calculated and expressed as a percentage of the control group (untreated cells). For concentration-response experiments, a dose-response curve was plotted to determine the half-maximal inhibitory concentration (IC50) of a given treatment, if applicable.

Ethynyl deoxyuridine (EdU) for Cell proliferation measurement

Cell Culture and Treatment: NPC cells were seeded in appropriate culture dishes or plates, depending on the scale of the experiment, and cultured under standard conditions (37°C, 5% CO_2). After 24 hours of cultivation, or at the specific time point relevant to the experimental design, the cells were ready for EdU labeling.

EdU Labeling: Ethynyl Deoxyuridine (EdU) is a thymidine analog that gets incorporated into DNA during active DNA synthesis, marking cells that are in the S-phase of the cell cycle. For the labeling, cells were incubated with EdU at a concentration recommended by the BeyoClick™ Edu-555 kit (Beyotime Institute of Biotechnology) protocol. The incubation period for EdU labeling is typically 1-2 hours, but this may vary depending on the cell type and proliferation rate.

Fixation and Permeabilization: Following the EdU incubation, cells were washed with PBS and fixed with 4% paraformaldehyde for 15 minutes to preserve cellular structures and DNA. Cells were then permeabilized with 0.5% Triton X-100 in PBS for 20 minutes to allow entry of the detection reagents.

EdU Detection: The BeyoClick™ Edu-555 kit employs a click chemistry reaction that specifically reacts with the alkyne group of EdU. This reaction was performed according to the manufacturer's instructions. It typically involves adding a reaction cocktail containing the fluorescent azide (in this case, a 555 fluorophore), a copper catalyst, and a buffer solution to the cells. The reaction was allowed to proceed for 30 minutes at room temperature in the dark.

Nuclear Staining: After the click reaction, nuclei were stained with a DNA dye, such as DAPI (4',6-diamidino-2-phenylindole), for visualization of all nuclei. The staining with DAPI allows for the identification of total cells, irrespective of their proliferation status.

Fluorescence Microscopy and Image Acquisition: The stained cells were washed with PBS and mounted for fluorescence microscopy. Cells were observed under a fluorescence microscope equipped with the appropriate filters for the Edu-555 and DAPI fluorophores. Images were captured from multiple fields to ensure a representative sample of the cell population.

Quantification and Data Analysis: The captured images were analyzed using Image J software (NIH, USA). The ratio of Edu-positive (proliferating) cells to the total number of nuclei (DAPI-stained) was calculated. This ratio provides an estimate of the proliferation rate within the cell population. The percentage of EdU-positive cells was calculated for each experimental condition and compared to controls.

Wound-healing migration assay

Cell Culture and Seeding: NPC cells were cultured under standard conditions (37°C in a

humidified atmosphere with 5% CO_2) in an appropriate growth medium. Once the cells reached optimal confluence (usually 90-100%), they were seeded into 6-well plates. The seeding density was chosen to ensure a monolayer formation without overcrowding, typically around 2-3 million cells per well, depending on the cell line.

Wound Creation: After the cells reached 100% confluence, creating a monolayer, a 'wound' was created in the cell monolayer. This was done using a sterile pipette tip (usually 200 µL) to scratch a straight line across the well. Care was taken to ensure that the width and depth of the scratch were consistent across all wells. The detached cells and debris were then gently washed away with phosphate-buffered saline (PBS).

Migration Period and Conditions: Following the creation of the wound, cells were incubated in serum-free medium or a medium with reduced serum content to minimize cell proliferation, which could confound the results of the migration assay. The cells were then allowed to migrate into the wound area for a fixed period, typically 48 hours. The incubation conditions were maintained as before.

Photographic Documentation: To assess cell migration, photographs of the wound were taken immediately after the scratch (0 hours) and at the end of the migration period (48 hours post-scratch). A microscope equipped with a camera was used, and images were captured at consistent magnification and lighting conditions. Marking the bottom of the well with a reference point ensured that images were taken at the same field of view.

Analysis of Wound Closure: The images were analyzed to calculate the rate of wound closure. This involved measuring the width of the wound at different time points using image analysis software, such as Image J. The percentage of wound closure was calculated by comparing the initial wound width (0 hours) with the wound width at 48 hours. The formula used was: Wound Closure% = ((Initial Width - Width at 48 hours)/(Initial Width)) × 100.

Colony formation experiment

Cell Preparation and Seeding: After 24 hours of culturing the transfected cells, they were prepared for the colony formation assay. The transfected cells were trypsinized, counted, and reseeded at a low density (typically 500-1000 cells per well) into 6-well plates. The low seeding density is crucial to ensure that each colony originates from a single cell, allowing for the assessment of the cell's ability to grow into a colony.

Colony Growth Conditions: The cells were incubated under standard culture conditions (37°C with 5% CO_2) and allowed to grow for a period sufficient to form visible colonies. This period generally ranged from 1 to 3 weeks, depending on the growth rate of the specific cell line. The culture medium was replaced every 3-4 days to provide fresh nutrients and maintain optimal growth conditions.

Staining and Visualization of Colonies: After the incubation period, when colonies were visibly formed, the medium was removed, and the cells were gently washed with phosphate-buffered saline (PBS). The colonies were fixed with a fixing solution, such as methanol or formaldehyde, for 15 minutes at room temperature. Following fixation, the cells were stained with 0.1% crystal violet solution for 30 minutes to 1 hour. The crystal violet dye binds to the DNA and proteins in the cells, staining the colonies a deep purple color. Excess stain was gently washed off with tap water.

Counting of Colonies: The stained plates were air-dried, and colonies containing more than 30 cells were counted. The threshold of 30 cells was set to distinguish true colonies from random cell clusters. Counting could be done manually or using an automated colony counter. The number of colonies in each well was recorded.

Data Analysis: The colony formation efficiency was calculated using the formula: Colony Formation Efficiency (%) = ((Number of colonies formed)/(Number of cells seeded)) × 100.

This efficiency indicates the cell's ability to survive and form a colony, reflecting the clonogenic potential of the cells under study.

Transwell invasion and migration assay

Assay Preparation: Transwell chambers with a pore size of 8 µm (Corning, NY, USA) were used for both invasion and migration assays. These chambers provide a physical barrier that cells

must actively move through, thus simulating the invasion or migration process.

Coating with Matrigel for Invasion Assays: For invasion assays, the upper compartment of the Transwell chambers was coated with Matrigel (BD Biosciences, San Jose, CA, USA) to simulate the extracellular matrix. Matrigel was diluted with serum-free medium to an appropriate concentration and added to the upper compartment. The coated chambers were incubated at 37°C for 4 hours to allow the Matrigel to solidify.

Cell Seeding: Cells were harvested and resuspended in a serum-free medium. For migration assays, approximately 1-2 × 10^5 cells were seeded into the upper compartment of each Transwell chamber. For invasion assays, the same number of cells was seeded into the Matrigel-coated chambers. The lower compartment was filled with medium containing a higher concentration of serum (10-20%) to serve as a chemoattractant, encouraging cells to migrate or invade through the membrane.

Incubation Period: The chambers were incubated at 37°C in a 5% CO_2 atmosphere. The incubation time varied depending on the cell type and the experimental requirements but generally ranged from 24 to 48 hours.

Staining and Visualization: After incubation, non-migrating or non-invading cells on the upper surface of the membrane were gently removed with a cotton swab. The cells that had migrated or invaded to the lower surface of the membrane were fixed with methanol for 15 minutes and stained with 0.1% crystal violet for 30 minutes. The stain binds to the DNA and proteins in the cells, making them visible for counting.

Counting Migrated/Invaded Cells: The stained cells on the lower surface of the membrane were counted under a light microscope. Counting was typically performed in five randomly selected fields per well to ensure an accurate representation of the cell migration or invasion.

Data Analysis: The average number of migrated or invaded cells was calculated for each experimental condition. These numbers were compared to control conditions to assess the relative migration or invasion capacity of the cells.

Cell cycle and apoptosis assays

Cell Preparation and Harvesting: NPC cells were cultured under optimal conditions until they reached the desired confluency. Before the assays, cells were harvested using trypsinization, neutralized with complete medium, and then washed with phosphate-buffered saline (PBS). The cell pellets were collected by centrifugation and counted to ensure a consistent number of cells for each assay.

Cell Cycle Analysis Using Cell Cycle Analysis Kit: Fixation: The cells were fixed in 70% ethanol at -20°C for at least 2 hours or overnight. This step is crucial for preserving cellular structures and halting all metabolic processes.

DNA Staining: After fixation, cells were washed to remove ethanol and treated with a DNA-staining solution containing propidium iodide (PI) and RNase. This solution stains the DNA of cells, allowing the quantification of DNA content in different phases of the cell cycle.

Flow Cytometry Analysis: The stained cells were then analyzed using a FACSCalibur flow cytometer. The PI fluorescence intensity correlates with the amount of DNA, enabling the distinction of cells in G0/G1, S, and G2/M phases of the cell cycle.

Apoptosis Analysis Using FITC-Annexin V/PI Apoptosis Detection Kit: Staining for Apoptosis: For apoptosis detection, cells were washed and then resuspended in a binding buffer. Following this, cells were stained with FITC-Annexin V and PI, as per the kit's protocol. FITC-Annexin V binds to phosphatidylserine on the outer leaflet of the plasma membrane of apoptotic cells, while PI stains the nuclei of cells with compromised membranes.

Flow Cytometry Analysis: The stained cells were subjected to flow cytometry using the FACSCalibur system. This analysis discriminates between live cells (Annexin V-/PI-), early apoptotic cells (Annexin V+/PI-), late apoptotic (Annexin V+/PI+), and necrotic cells (Annexin V-/PI+).

Data Acquisition and Interpretation: Data from the flow cytometer were acquired and analyzed using the associated software. A minimum of 10,000 cells per sample were recorded to ensure statistical robustness. Results were

quantified and expressed as the percentage of cells in different stages of the cell cycle or apoptosis.

Western blot

In this study, protein sample were meticulously prepared for analysis. Initially, proteins were extracted from the relevant cells or tissues. Following extraction, these proteins underwent separation through sodium dodecyl sulfate-polyacrylamide gel electrophoresis (SDS-PAGE).

Subsequent to the SDS-PAGE process, the separated proteins were carefully transferred onto polyvinylidene fluoride (PVDF) membranes. This transfer is crucial for the subsequent detection steps. The PVDF membranes, bearing the proteins, were then treated with a 5% solution of nonfat milk. This step is critical as it blocks nonspecific binding sites on the membrane, thereby enhancing the specificity of antibody binding in later stages.

The next phase involved the incubation of these membranes with a series of primary antibodies. These antibodies are designed to specifically bind to target proteins of interest. Following this primary antibody binding, the membranes were further incubated with horseradish peroxidase (HRP)-tagged secondary antibodies. These secondary antibodies are conjugated with an enzyme (HRP) that facilitates the detection of the primary antibody-protein complexes.

Finally, the visualization of these protein bands was achieved using an enhanced chemiluminescence (ECL) substrate. This substrate reacts with the HRP enzyme, producing a luminescent signal that can be detected and quantified. This signal directly corresponds to the presence and abundance of the target proteins, thus allowing for a thorough analysis of protein expression.

Fluorescence in situ Hybridisation (FISH)

In this study, a detailed analysis of cellular localization of the lncRNA EP300-AS1 was conducted using fluorescence in situ hybridization (FISH) (RiboBio, catalog number C10910) [23]. Initially, cells were fixed to preserve their structure and components. This step is critical as it immobilizes all cellular constituents, thereby maintaining their in situ positions and allowing for accurate localization studies.

Subsequently, these fixed cells were subjected to hybridization with a specifically designed FISH probe targeting EP300-AS1 (RiboBio). This probe is a fluorescently labeled oligonucleotide that specifically binds to the EP300-AS1 lncRNA sequence. The hybridization process facilitates the binding of the probe to its complementary sequence within the cellular RNA.

Following the hybridization, the cells were analyzed using a fluorescence microscope. This advanced imaging technique enabled the visualization of the fluorescent signals emitted by the bound FISH probe. The location and intensity of these signals within the cells provide valuable information about the distribution and abundance of the EP300-AS1 lncRNA.

This methodological approach is essential for understanding the spatial and temporal expression patterns of lncRNAs like EP300-AS1 in cells. It contributes significantly to elucidating their functional roles in cellular processes and can be instrumental in identifying potential targets for therapeutic interventions in diseases where lncRNAs are implicated.

Methylation-specific polymerase chain reaction

In the conducted experiment, a critical step involved the conversion of unmethylated cytosine residues in DNA to uracil. This transformation was accomplished using a DNA Bisulfite Conversion Kit, sourced from TIANGEN (catalog number DP215). The bisulfite conversion process is essential for the subsequent analysis of DNA methylation patterns, as it differentially alters unmethylated cytosine while leaving methylated cytosine unchanged.

Following this conversion, the bisulfite-treated DNA was subjected to polymerase chain reaction (PCR) amplification. This step was facilitated by employing a Methylation-Specific PCR Kit, also provided by TIANGEN (catalog number EM101) [24]. The PCR process selectively amplified the converted DNA, enabling the distinction between methylated and unmethylated alleles.

To achieve specificity in the PCR amplification, primers were meticulously designed and ob-

Table 2. Methylated and unmethylated primer sequences

Gene name	Primer sequence (5'-3')
CST6	Left M primer: TTTCGAGATACGTATATTATTAAGGC
	Right M primer: TTCATACACGCTAAAACAACG
	Left U primer: TTATTTTTGAGATATGTATATTATTAAGGT
	Right U primer: CCCTTCATACACACTAAAACAACAC

tained from GENERAL BIOL. These primers were tailored to recognize sequences in the bisulfite-converted DNA, allowing for the effective differentiation between methylated and unmethylated alleles. The design and selection of these primers were critical for the accuracy of the methylation analysis, and the details of these primers are outlined in **Table 2** of the manuscript.

Upon the completion of the PCR process, a 10 µl sample of the reaction mixture was collected for analysis. The assessment of this sample was conducted using agarose gel electrophoresis, a technique that allows for the visualization of DNA fragments based on their size. This method provided a clear representation of the PCR amplification products, enabling the evaluation of the efficiency and specificity of the methylation-specific PCR. This comprehensive approach is crucial for advancing our understanding of DNA methylation and its role in various biological processes and diseases.

Chromatin immunoprecipitation (ChIP) assay

In this study, we employed chromatin immunoprecipitation (ChIP) assays to investigate protein-DNA interactions [25], specifically focusing on the transcription factor AP-2 gamma (TFAP2C, ab218107, abcam). The ChIP assays were meticulously performed in accordance with the protocol provided by Beyotime (Kit P2078), ensuring high fidelity in the experimental procedures.

The initial phase of the assay involved treating cells with paraformaldehyde. This step is critical as it facilitates the creation of cross-links between DNA and the associated proteins, thereby preserving the interactions that occur within the cell's nucleus.

Subsequent to cross-linking, the cells were subjected to lysis, releasing the chromatin into solution. This chromatin was then fragmented into smaller pieces using sonication, a process that employs ultrasonic energy to break the DNA into segments of manageable size for immunoprecipitation.

Following sonication, the fragmented chromatin was incubated with two different antibodies: anti-TFAP2C and a control immunoglobulin G (IgG). The anti-TFAP2C antibody specifically binds to TFAP2C, allowing for the immunoprecipitation of DNA regions interacting with this transcription factor. In contrast, the control IgG serves as a negative control to assess non-specific binding.

After the incubation, the samples were subjected to centrifugation at 4°C for an extended period. This step separates the antibody-bound DNA-protein complexes from the rest of the chromatin.

The next critical step involved reversing the DNA-protein cross-links, a process that liberates the DNA from the protein. Once free, the chromatin DNA was extracted and purified, preparing it for subsequent analysis.

After the ChIP procedure, we used quantitative real-time PCR (qPCR) to quantify the enrichment of TFAP2C-bound DNA fragments. The relative enrichment of the target regions was calculated using the $2^{-\Delta\Delta Ct}$ method, comparing the ChIP samples to input DNA controls [26]. This approach allowed us to precisely measure the degree of TFAP2C binding at specific genomic loci. To ensure the reliability of our qPCR results, we included multiple biological replicates (n = 3) for each condition. The consistency observed across these replicates strengthens the validity of our conclusions regarding TFAP2C binding.

The final stage of the assay involved the separation of the amplified PCR products on a 1% agarose gel. Agarose gel electrophoresis is a widely-used technique for the resolution of DNA fragments, based on their size. Following electrophoresis, the separated DNA bands were photographed. This visual representation provides a clear indication of the presence and size of the PCR products, reflecting the DNA sequences that were associated with TFAP2C in the cells.

Through this comprehensive ChIP assay protocol, we were able to effectively isolate and ana-

lyze the DNA regions interacting with TFAP2C, shedding light on the genomic binding sites of this key transcription factor. This approach is invaluable in the study of gene regulation mechanisms, contributing to a deeper understanding of cellular processes.

RNA pull - down assay

In this investigation, we utilized the RNA pull-down assay, a technique pivotal for elucidating RNA-protein interactions. This assay was conducted using the FITGENE RNA Pull-down Kit (catalog number FI88702) [27], with strict adherence to the manufacturer's guidelines to ensure accuracy and reproducibility.

The first step of the assay involved the construction of the target RNA, designated as RNA-F2. This synthetic RNA was carefully designed to mirror the sequence of interest in our study. Following its synthesis, RNA-F2 was introduced into NPC cells via transfection. This process enabled the RNA-F2 to interact with endogenous RNA-binding proteins within these cells, forming RNA-protein complexes essential for the subsequent steps of the assay.

After sufficient time for interaction, the NPC cells were lysed. Cell lysis is a crucial step as it releases the RNA-protein complexes into the lysate, allowing for their isolation and analysis. The lysate was then subjected to a pull-down procedure using ligands specific to RNA-F2. These ligands were attached to magnetic beads, facilitating the selective capture of RNA-F2 and any associated RNA-binding proteins.

Once the target RNA and its bound proteins were immobilized on the magnetic beads, the beads were washed to remove non-specifically bound components. This step is vital for the specificity and clarity of the subsequent analysis.

The final stage involved the elution of the RNA-protein complexes from the magnetic beads. These eluted complexes were then analyzed using western blotting. Western blot is a robust technique for detecting specific proteins within a sample. By applying this method, we were able to identify and characterize the proteins that specifically interact with RNA-F2 in NPC cells.

Through this RNA pull-down assay, we gained valuable insights into the interaction dynamics between RNA-F2 and its binding proteins in NPC cells. Such studies are instrumental in understanding the roles of RNA-protein complexes in cellular processes, potentially paving the way for novel therapeutic strategies in the treatment of nasopharyngeal carcinoma.

Animal studies

In our study, we focused on establishing NPC xenografts using a well-established animal model. Four-week-old BALB/c nude mice, procured from the Experimental Animal Center of Hainan Medical University, were chosen for this purpose due to their immunodeficient status, which allows for the successful engraftment of human cells.

The mice were injected subcutaneously with cells that had been stably transfected. This transfection process ensured that the cells carried specific genetic modifications, crucial for the study of tumor biology in the context of NPC. The subcutaneous injection was chosen as it facilitates the formation of solid tumors at predictable and accessible sites on the mice.

Following the injection, we diligently monitored the tumor growth in these mice over time. Tumor volume was measured at regular intervals using calipers, a non-invasive method that provides an accurate assessment of tumor size. This monitoring was crucial for evaluating the progression of the xenografts and for determining the appropriate timing for subsequent experimental interventions.

It is imperative to note that all animal experiments conducted in this study were approved by the Animal Ethics Committee of the First Affiliated Hospital of Hainan Medical University. This approval underscores our commitment to ethical research practices and the welfare of the animals used in our study. Furthermore, our experimental procedures were in strict compliance with the National Institutes of Health guide for the care and use of laboratory animals. Adhering to these guidelines ensured that the mice were housed and handled in a manner that prioritizes their well-being and minimizes distress, thereby maintaining the integrity of the experimental results.

This approach of using NPC xenografts in BALB/c nude mice serves as a critical model for understanding tumor development and progression, and it provides a valuable platform for testing therapeutic interventions in nasopharyngeal carcinoma.

Statistical analysis

All statistical analyses were conducted using SPSS software, version 20.0. The data obtained from these experiments are presented as the mean ± standard deviation (SD). For numerical variables, we conducted statistical tests based on the data distribution. If the data met the criteria for a normal distribution and passed the homogeneity of variance test, we used the t-test for comparisons between two groups and One-way ANOVA for comparisons among three or more groups. If the data were normally distributed but failed the homogeneity of variance test, we applied Welch's t-test for two-group comparisons and Welch's One-way ANOVA for three-group comparisons. For data that did not meet the criteria for normal distribution, we utilized the Wilcoxon rank-sum test (Mann-Whitney U test) for two-group comparisons and the Kruskal-Wallis H test for three-group comparisons.

For categorical variables, we employed the Chi-square test for inter-group com-parisons when all expected frequencies were greater than 5 and the total sample size was 40 or more. When expected frequencies ranged from 1 to 5 with a total sample size of 40 or more, we used the Chi-square test with continuity correction (Yates' correction). In cases where the expected frequency was less than 1 or the total sample size was below 40, we used Fisher's exact test for inter-group comparisons. A *p*-value of less than 0.05 was considered statistically significant. For survival studies, the Kaplan-Meier analysis was employed.

Results

lncRNA EP300-AS1 gene expression analysis in diverse cancer contexts

Expression patterns across cancer types: Our findings, as shown in **Figure 1A**, revealed that EP300-AS1 expression is significantly higher in cervical and endocervical cancers (CESC), glioblastoma multiforme (GBM), prostate adenocarcinoma (PRAD), and kidney clear cell carcinoma (KIRC) compared to normal samples. In contrast, its expression is notably lower in lung squamous cell adenocarcinoma (LUSC), lung adenocarcinoma (LUAD), thyroid carcinoma (THCA), and rectum adenocarcinoma (READ) compared to adjacent normal tissues.

Head and neck squamous cell carcinoma analysis: Both paired and unpaired analyses of HNSC consistently demonstrated that lncRNA EP300-AS1 is underexpressed in tumor samples compared to normal tissue (**Figure 1B** and **1C**). We further validated this trend by conducting gene association studies and identified the top 100 genes most significantly associated with EP300-ASI (Table S1), with C5orf66, HLF, PDK1L, LRRC8B, and CYB5RL being the most prominent (**Figure 1D**).

Expression in nasopharyngeal carcinoma: Analysis from the GEO datasets GSE12452 (**Figure 1E**) and GSE64634 (**Figure 1F**) revealed that lncRNA EP300-AS1 exhibits low expression in NPC, a finding that was further supported by comparisons with NPC cell lines (5-8F and CNE1) (**Figure 1G**).

lncRNA EP300-AS1 expression as a potential diagnostic biomarker in HNSC patient: ROC analysis of the TCGA-HNSC dataset revealed an estimated Area Under the Curve (AUC) of 0.698 (95% CI: 0.623-0.773), as depicted in **Figure 1H**. This AUC value indicates that EP300-AS1 has a moderate discriminatory ability in differentiating HNSC from normal tissue.

The AUCs for lncRNA EP300-AS1 in the GSE12452 and GSE64634 datasets were 0.952 (95% CI: 0.876-1.000, **Figure 1I**) and 0.875 (95% CI: 0.619-1.000, **Figure 1J**), respectively. These higher AUC values suggest a strong diagnostic potential of EP300-AS1 expression in distinguishing HNSC from normal tissues. Moreover, in certain cancer datasets, EP300-AS1 demonstrates significant potential as a biomarker, with a AUC value exceeding 0.9 - an indicator typically considered excellent [28].

Our comprehensive ROC analysis across multiple datasets supports the potential of lncRNA EP300-AS1 expression as a reliable diagnostic biomarker in HNSC patients. The variation in AUC values across different datasets empha-

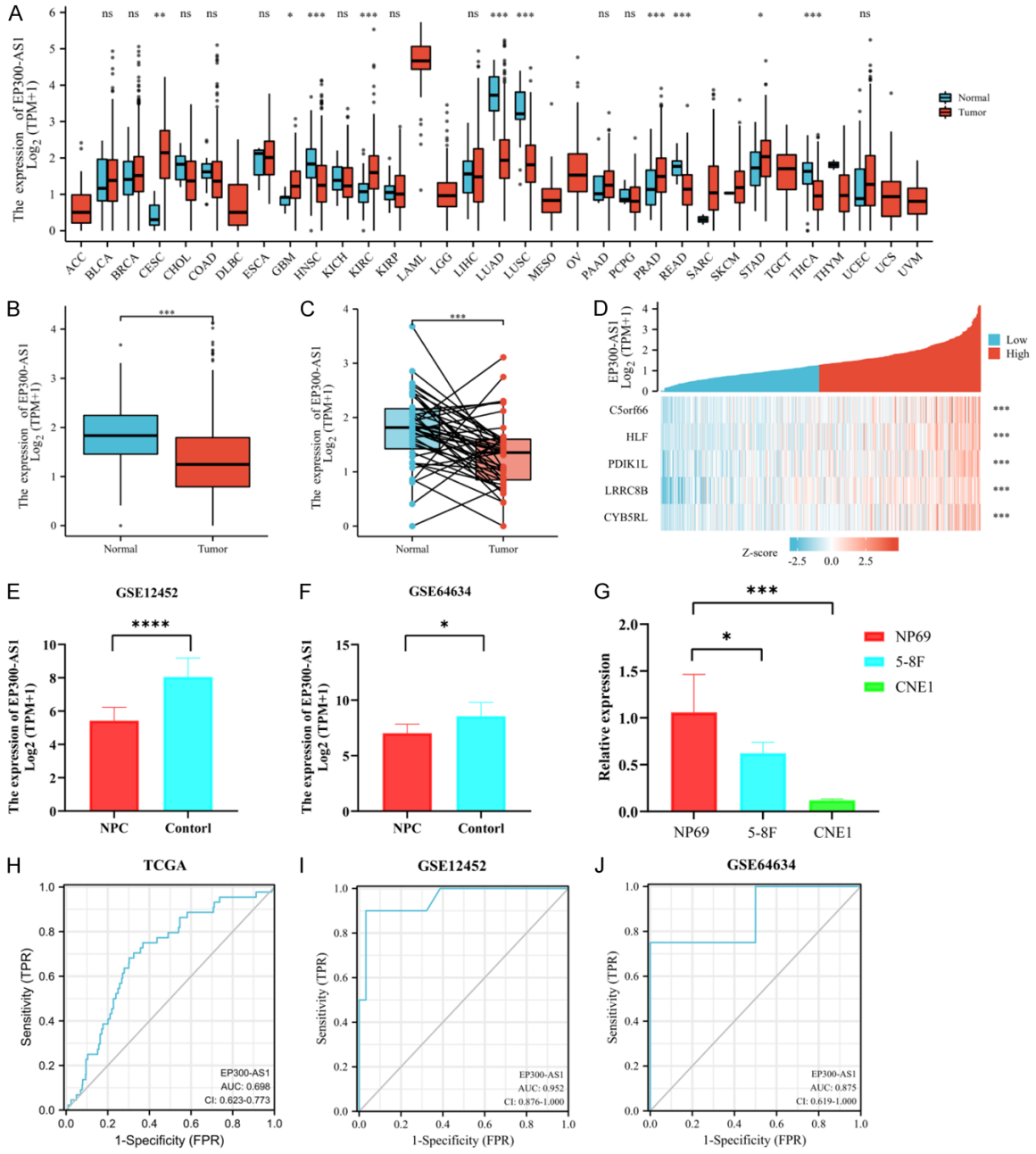

Figure 1. Differential expression of lncRNA EP300-AS1 across varied cancer tissues. A. By employing The Cancer Genome Atlas (TCGA), the levels of lncRNA EP300-AS1 mRNA expression were evaluated across a diversity of tumor and normal tissues. B. The TCGA-HNSC datasets revealed a substantial downregulation of lncRNA EP300-AS1 mRNA expression in head and neck squamous cell carcinoma (HNSC) tumor tissues compared to normal tissues. C. These datasets further showed a significant reduction in the expression of lncRNA EP300-AS1 in paired HNSC tumor tissues relative to adjacent normal tissues. D. Heatmaps represent the expression levels of specific mRNAs in HNSC patients with high and low lncRNA EP300-AS1 expression (n = 546), based on the TCGA-HNSC project. E, F. Both GSE12452 and GSE64634 datasets exhibited considerably reduced lncRNA EP300-AS1 mRNA expression in nasopharyngeal cancer compared to normal tissues. G. The mRNA expression levels of lncRNA EP300-AS1 were assessed in NPC cell lines (CNE1 and 5-8F) and normal nasopharyngeal cell lines (NP69). H. A receiver operating characteristic (ROC) analysis using the TCGA-HNSC datasets indicated that lncRNA EP300-AS1 expression can reliably distinguish HNSC tumor tissues from normal tissues, with an area under the curve (AUC) of 0.698 (95% CI = 0.623-0.773). I, J. ROC analyses conducted with GSE12452 and GSE64634 datasets showed that lncRNA EP300-AS1 expression accurately differentiates nasopharyngeal cancer tissues from normal tissues, achieving AUCs of 0.952 (95% CI = 0.876-1.000) and 0.875 (95% CI = 0.619-1.000), respectively.

sizes the importance of considering diverse patient populations and experimental conditions in biomarker validation studies.

lncRNA EP300-AS1 expression as a poor prognosis in HNSC patients and functional enrichment

Survival analysis and prognostic significance: In the TCGA-HNSC dataset, the Kaplan-Meier survival analysis suggested a strong correlation between low lncRNA EP300-AS1 expression and decreased overall survival (OS), progression-free interval (PFI), and disease-specific survival (DSS) in HNSC patients (**Figure 2A-C**). These findings were further validated using the GEO database, which showed that poor prognosis in OS (HR = 0.66, P = 0.0027, **Figure 2D**) and disease-free survival (DFS) (HR = 0.68, P = 0.026, **Figure 2E**) was associated with reduced lncRNA EP300-AS1 expression, strengthening our initial observations. Univariate and multivariate Cox regression analyses identified that the expression level of lncRNA EP300-AS1, N stage, and M stage, were independent predictors of OS in HNSC patients (**Table 3**).

Functional enrichment analysis: After enriching the 100 genes associated with lncRNA EP300-AS1, the most prevalent biological processes identified were signal transduction by DNA replication, p53 class mediator, regulation of DNA repair, and response to DNA damage stimulus regulation (Table S2). Regarding cell components, the majority included the PcG protein complex, tight junction, ESC/E(Z) complex, H4/H2A histone acetyltransferase complex, and NuA4 histone acetyltransferase complex. The KEGG pathway analysis suggested that lncRNA EP300-AS1 plays a crucial role in various cancer cells (**Figure 2F**).

These findings highlight lncRNA EP300-AS1's potential regulatory function within the nucleus of cancer cells, emphasizing its influence on the pathophysiology and progression of HNSC.

The tumor suppressor lncRNA EP300-AS1 functions in nasopharyngeal carcinoma

Initial construction and transfection efficiency assessment: To begin our experiment, we constructed the lncRNA EP300-AS1 overexpression plasmid and evaluated its ability to transfect NPC cell lines. We achieved a transfection efficiency surpassing 60% (refer to Figure S1A-D), providing a solid foundation for subsequent in-depth analyses.

Effects of overexpression on cell growth: In our study, we evaluated the impact of the long non-coding RNA EP300-AS1 on the growth of nasopharyngeal carcinoma (NPC) cell lines CNE1 and 5-8F by overexpressing EP300-AS1. Initially, EdU incorporation assays were performed to assess cell proliferation, and immunofluorescence staining was used to visually demonstrate the proliferative status of the cells (**Figure 3A**). Statistical analysis of the EdU-positive cells (**Figure 3B**) confirmed that EP300-AS1 overexpression significantly decreased the proliferation of these cancer cells.

To further investigate the sustained effects of EP300-AS1 overexpression, we conducted CCK8 assays to monitor cell viability over time (**Figure 3C**). The results showed a substantial reduction in cell viability in the EP300-AS1 overexpression group compared to the control group, indicating that EP300-AS1 exerts a prolonged inhibitory effect on NPC cell proliferation. Collectively, these findings demonstrate that overexpression of EP300-AS1 significantly suppresses the growth of NPC cells.

Impact on cell line migration, cloning, and invasiveness: To comprehensively assess the impact of EP300-AS1 overexpression on cellular behavior, we began with scratch wound healing assays (Figure S2A) to evaluate cell migration. Our results revealed that EP300-AS1 overexpression significantly slowed migration in both CNE1 and 5-8F nasopharyngeal carcinoma cell lines. Specifically, after 48 hours, the wound area was markedly smaller in the EP300-AS1 overexpression group compared to the negative control, underscoring its inhibitory effect on migration.

Next, we assessed clonogenic potential using soft agar colony formation assays (Figure S2B). The data showed a significant reduction in both the number and size of colonies formed by CNE1 and 5-8F cells upon EP300-AS1 overexpression, indicating a strong suppressive effect on clonogenic capacity and further supporting its role in regulating cancer progression.

Additionally, Transwell migration and invasion assays (Figure S2C, S2D) were performed to

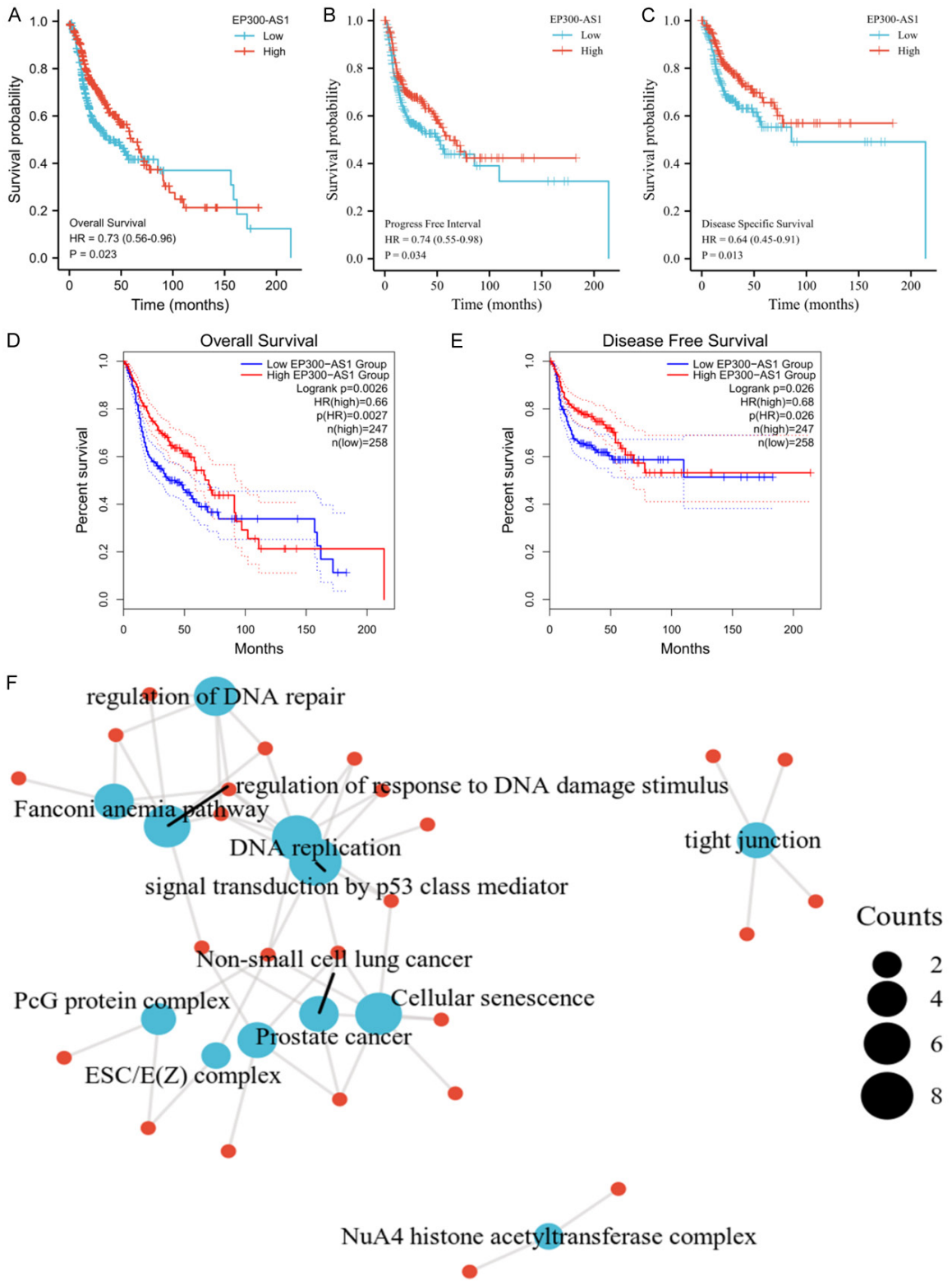

Figure 2. Evaluating the prognostic significance and role of lncRNA EP300-AS1 in HNSC. A-C. Survival curves drawn from the TCGA-HNSC datasets illustrate OS, PFI, and DSS rates among HNSC patients with either low or high expression of lncRNA EP300-AS1. D, E. lncRNA EP300-AS1 expression levels in HNSC were analyzed using the GEPIA2.0 database to gauge its impact on OS and disease-free survival (DFS) rates. F. The Gene Ontology (GO) and Kyoto Encyclopedia of Genes and Genomes (KEGG) visualization network was used to understand the functional implications of lncRNA EP300-AS1.

Table 3. Univariate and multivariate analysis of the clinicopathological factors associated with the OS of patients with head and neck squamous cell carcinoma (HNSC)

Characteristics	Total (N)	Univariate analysis		Multivariate analysis	
		Hazard ratio (95% CI)	*P* value	Hazard ratio (95% CI)	*P* value
Age	501				
≤60	245	Reference			
>60	256	1.252 (0.956-1.639)	0.102		
Gender	501				
Female	134	Reference			
Male	367	0.764 (0.574-1.018)	0.066	0.807 (0.600-1.087)	0.158
T stage	486				
T1 & T2	176	Reference			
T3 & T4	310	1.245 (0.932-1.661)	0.137		
N stage	479				
N0 & N1	318	Reference			
N2 & N3	161	1.384 (1.040-1.842)	0.026	1.435 (1.068-1.928)	0.016
M stage	476				
M0	471	Reference			
M1	5	4.745 (1.748-12.883)	0.002	3.929 (1.434-10.770)	0.008
Clinical stage	487				
Stage I & Stage II	113	Reference			
Stage III & Stage IV	374	1.217 (0.878-1.688)	0.238		
Smoker	491				
No	111	Reference			
Yes	380	1.089 (0.778-1.525)	0.618		
Histologic grade	482				
G1 & G2	361	Reference			
G3 & G4	121	0.939 (0.688-1.282)	0.692		
Alcohol history	490				
No	158	Reference			
Yes	332	0.952 (0.716-1.265)	0.733		
EP300-AS1	501	0.739 (0.612-0.891)	0.002	0.726 (0.598-0.880)	0.001

explore the effects on cell migration and invasion. These experiments demonstrated a pronounced decrease in the number of migrated and invaded cells in both cell lines with EP300-AS1 overexpression compared to controls. Collectively, these findings indicate that EP300-AS1 overexpression not only impedes cell migration and clonogenicity but also significantly reduces the invasive capabilities of NPC cells.

Apoptotic response and protein expression changes: To elucidate the role of EP300-AS1 in apoptosis, we conducted a series of analyses using flow cytometry and Western blotting. Flow cytometry results (**Figure 3D**) revealed that overexpression of EP300-AS1 significantly increased the proportion of cells undergoing early apoptosis compared to the control group, suggesting that EP300-AS1 plays a crucial role in initiating apoptosis in NPC cells.

Complementing these findings, Western blot analysis (**Figure 3E**) showed that EP300-AS1 overexpression markedly upregulated pro-apoptotic proteins such as Bax and Caspase-3 while significantly downregulating the anti-apoptotic protein Bcl-2. This modulation of key apoptotic regulators indicates that EP300-AS1 promotes apoptosis by finely tuning the balance between pro-apoptotic and anti-apoptotic factors.

Collectively, these observations further support the potential of EP300-AS1 as a therapeutic target in NPC.

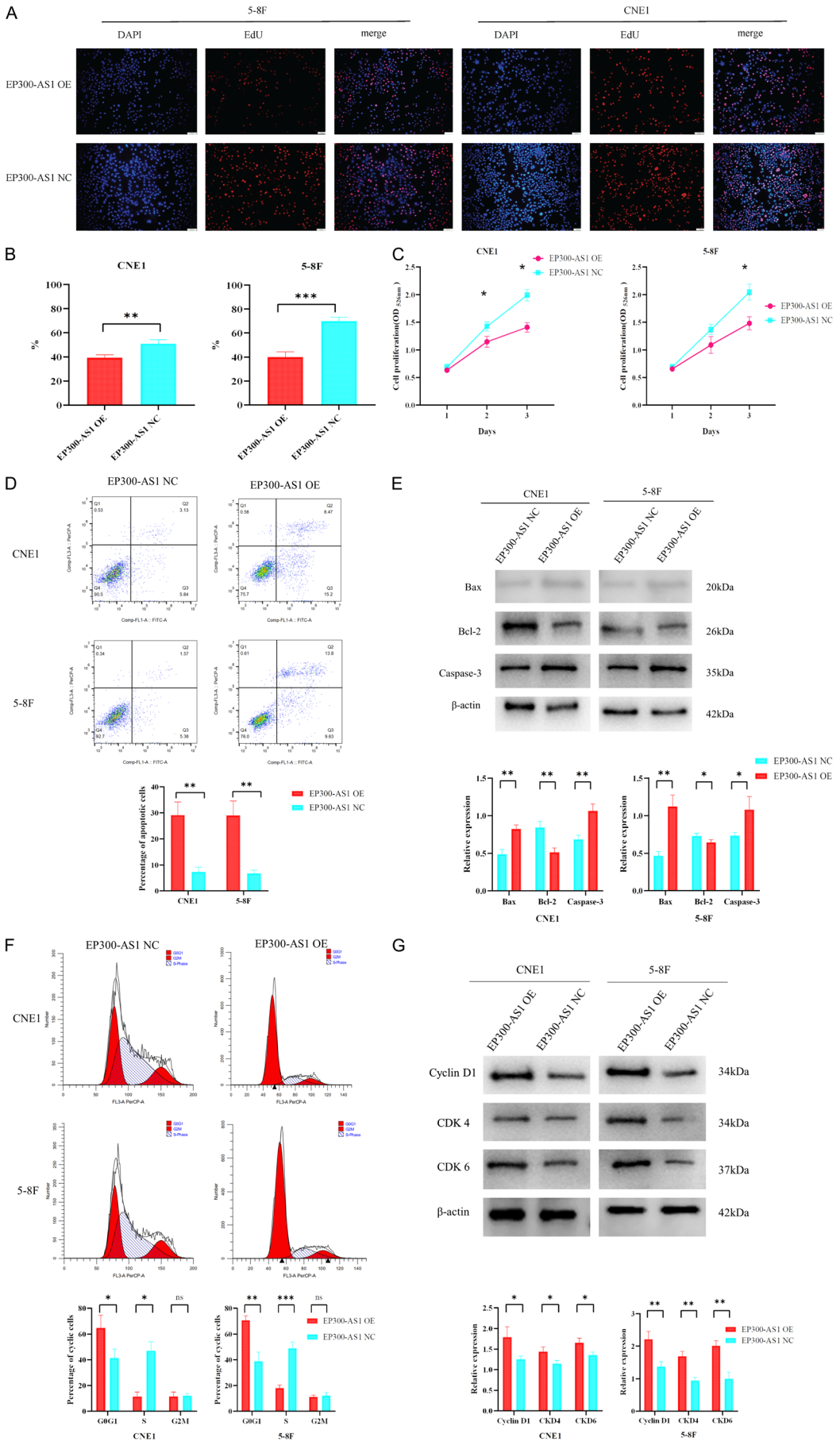
A
5-8F
CNE1
DAPI
EdU
merge
EP300-AS1 OE
EP300-AS1 NC
B
CNE1
5-8F
%
EP300-AS1 OE
EP300-AS1 NC
C
CNE1
5-8F
Cell proliferation(OD 450nm)
Days
EP300-AS1 OE
EP300-AS1 NC
D
EP300-AS1 NC
EP300-AS1 OE
CNE1
5-8F
Percentage of apoptotic cells
E
CNE1
5-8F
Bax
Bcl-2
Caspase-3
β-actin
20kDa
26kDa
35kDa
42kDa
Relative expression
F
EP300-AS1 NC
EP300-AS1 OE
CNE1
5-8F
Percentage of cyclic cells
G0G1
S
G2M
G
CNE1
5-8F
Cyclin D1
CDK 4
CDK 6
34kDa
34kDa
37kDa
42kDa
Relative expression
CKD4
CKD6

Figure 3. Overexpression of lncRNA EP300-AS1 inhibits proliferation, migration, cloning, and invasion of NPC cell lines. NPC cell lines (CNE1 and 5-8F cells) were transfected with pEGFP-C1 and pEGFP-C1- lncRNA EP300-AS1. A, B. EdU incorporation assays were conducted to evaluate cell proliferation in control NPC cells and in cells with stable overexpression of lncRNA EP300-AS1. Red staining signifies proliferating cells and EdU-positive nuclei. C. CCK8 assays were employed to assess cell proliferation in control NPC cells and in cells overexpressing lncRNA EP300-AS1. Cell proliferation was gauged by optical density (OD) readings at 450 nm. D. Overexpression of lncRNA EP300-AS1 triggers apoptosis in NPC cells. E. Examination of changes in expression of apoptotic genes (Bax, Bcl-2, and Caspase-3) upon overexpression of lncRNA EP300-AS1. F. Overexpression of lncRNA EP300-AS1 alters cell cycle distribution in NPC cells. The red tall regions represent the G0/G1 phase, while the low flat regions represent the G2/M phase. G. lncRNA EP300-AS1 induces an increase in the expression of G0/G1 phase proteins (Cyclin D1, CDK4, and CDK6). Scale bars = 100 μm.

Cell cycle modulation: Our cell cycle analysis revealed that overexpressing lncRNA EP300-AS1 led to a reduction of cells in the S-phase, with a concomitant increase in cells arrested in the G0/G1 phase (**Figure 3F**). This shift was associated with an elevated expression of specific G0/G1-phase proteins, including Cyclin D1, CDK4, and CDK6, as depicted in **Figure 3G**.

Our comprehensive study demonstrates that lncRNA EP300-AS1 acts as a potent suppressive agent in NPC. It impedes cell proliferation, migration, and cloning capabilities, disrupts normal cell cycle progression, and promotes apoptotic processes.

Role of lncRNA EP300-AS1 in NPC: in vivo studies and EMT signaling modulation

In vivo analysis of lncRNA EP300-AS1 in NPC development: To investigate the role of lncRNA EP300-AS1 in NPC progression, we conducted in vivo studies. We subcutaneously inoculated nude mice with NPC cell lines CNE1 and 5-8F, which were genetically modified to overexpress lncRNA EP300-AS1. The results, presented in **Figure 4A-C**, showed a significant reduction in the growth of xenograft tumors due to lncRNA EP300-AS1 overexpression.

Downstream protein expression modulation: In our exploration of the molecular pathways influenced by lncRNA EP300-AS1, a notable increase was observed in the expression of the downstream protein CST6 upon its overexpression (**Figure 4D**). Previous studies have identified CST6 as a crucial modulator in head and neck squamous cell carcinoma (HNSC), where it inhibits proliferation and EMT, while promoting epithelial cell characteristics [16].

Impact on EMT marker expression in NPC cells: We further investigated the expression of EMT markers in the transfected NPC cell lines. Our results demonstrated that lncRNA EP300-AS1 overexpression led to a downregulation of mesenchymal markers, including Vimentin, N-cadherin, and Snail, and a simultaneous upregulation of the epithelial marker E-cadherin (**Figure 4E**). This suggests a critical role of lncRNA EP300-AS1 in driving NPC cells towards an epithelial phenotype.

Validation in animal models: The in vivo model provided supporting evidence for our cellular findings. In mice overexpressing lncRNA EP300-AS1, CST6 expression mirrored the in vitro results, showing a consistent upregulation (**Figure 4F**). Moreover, the expression patterns of EMT markers in these mice were consistent with our in vitro observations: N-cadherin, Vimentin, and Snail expressions were reduced, while E-cadherin expression was increased (**Figure 4G**). Our study sheds light on the role of lncRNA EP300-AS1 in inhibiting NPC tumor growth. This suppression mechanism appears to operate through the modulation of CST6 expression, which subsequently inhibits cell proliferation and hinders the EMT process.

Elucidating the mechanism of lncRNA EP300-AS1 in Regulating CST6 via TFAP2C targeting

Subcellular localization and implications in cancer biology: To understand how lncRNA EP300-AS1 regulates CST6, we conducted a subcellular study, which revealed a predominant presence of lncRNA EP300-AS1 in the nucleus (**Figure 5A**). Transcriptional perturbations caused by molecular factors pose a significant challenge in cancer biology. Disturbances within gene regulatory networks play a significant role in the onset and advancement of cancer. Through the systematic development of a comprehensive Pan-cancer LncRNA Modulator Atlas (lncMAP), diverse categories of lncRNA regulatory agents have been pinpointed. These molecules are expressed across mul-

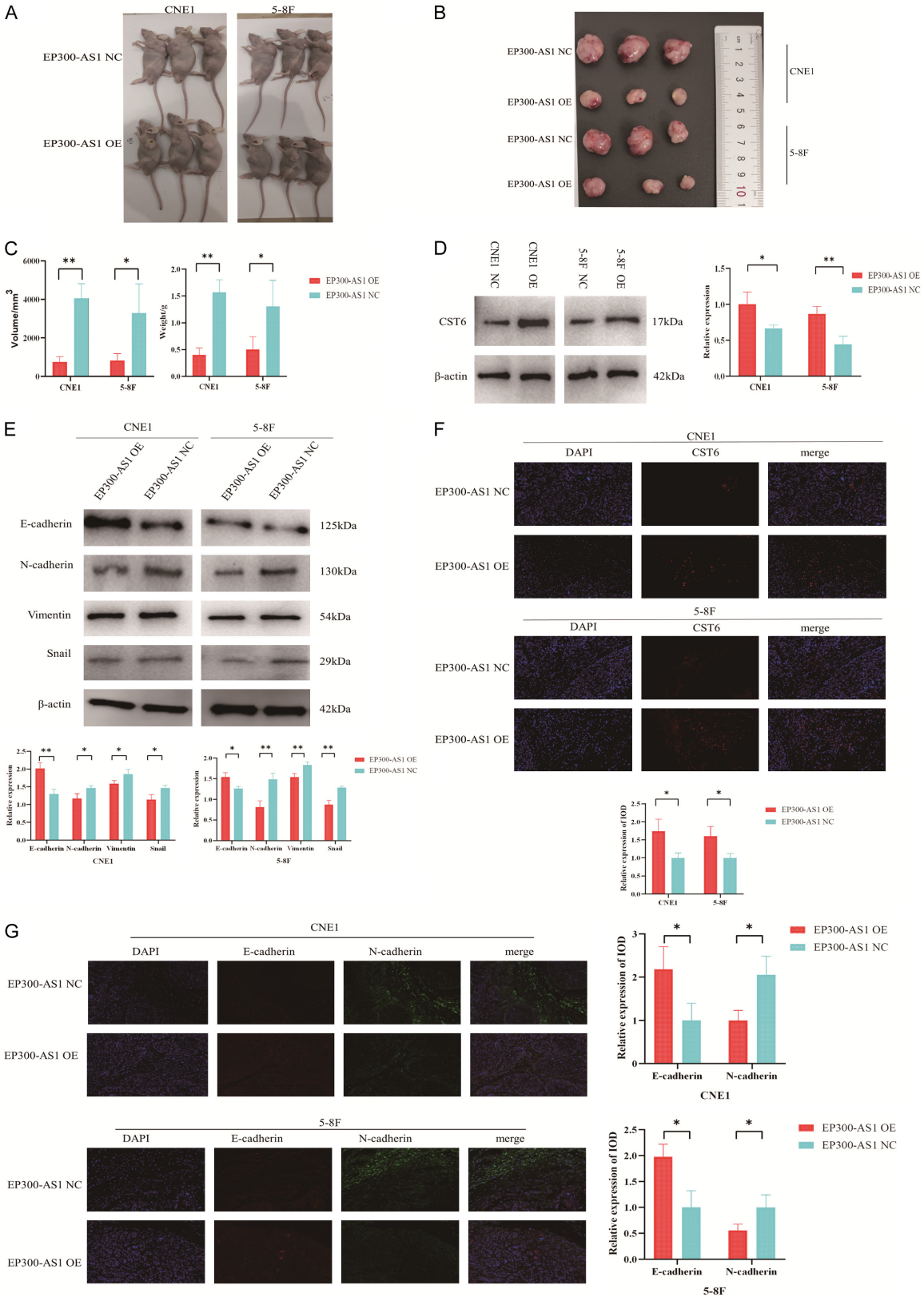

Figure 4. LncRNA EP300-AS1 Suppresses Tumor Progression by Modulating CST6. A, B. Overexpression of lncRNA EP300-AS1 in nude mice is shown before and after tumor extraction 28 days post-tumor induction. C. Mice were euthanized on the 28th day post-inoculation, with subcutaneous tumors being excised, volumes measured, and

individual animal weights recorded. D. LncRNA EP300-AS1 enhances CST6 expression. E. Overexpression of lncRNA EP300-AS1 bolsters E-cadherin expression and curbs the expression of N-cadherin, Vimentin, and Snail in CNE1 and 5-8F cell lines. F. LncRNA EP300-AS1 modulates CST6 expression during tumor formation in nude mice. G. LncRNA EP300-AS1 controls the expression of EMT markers (E-cadherin, N-cadherin, Vimentin, and Snail) during tumorigenesis in nude mice. Scale bars = 100 μm.

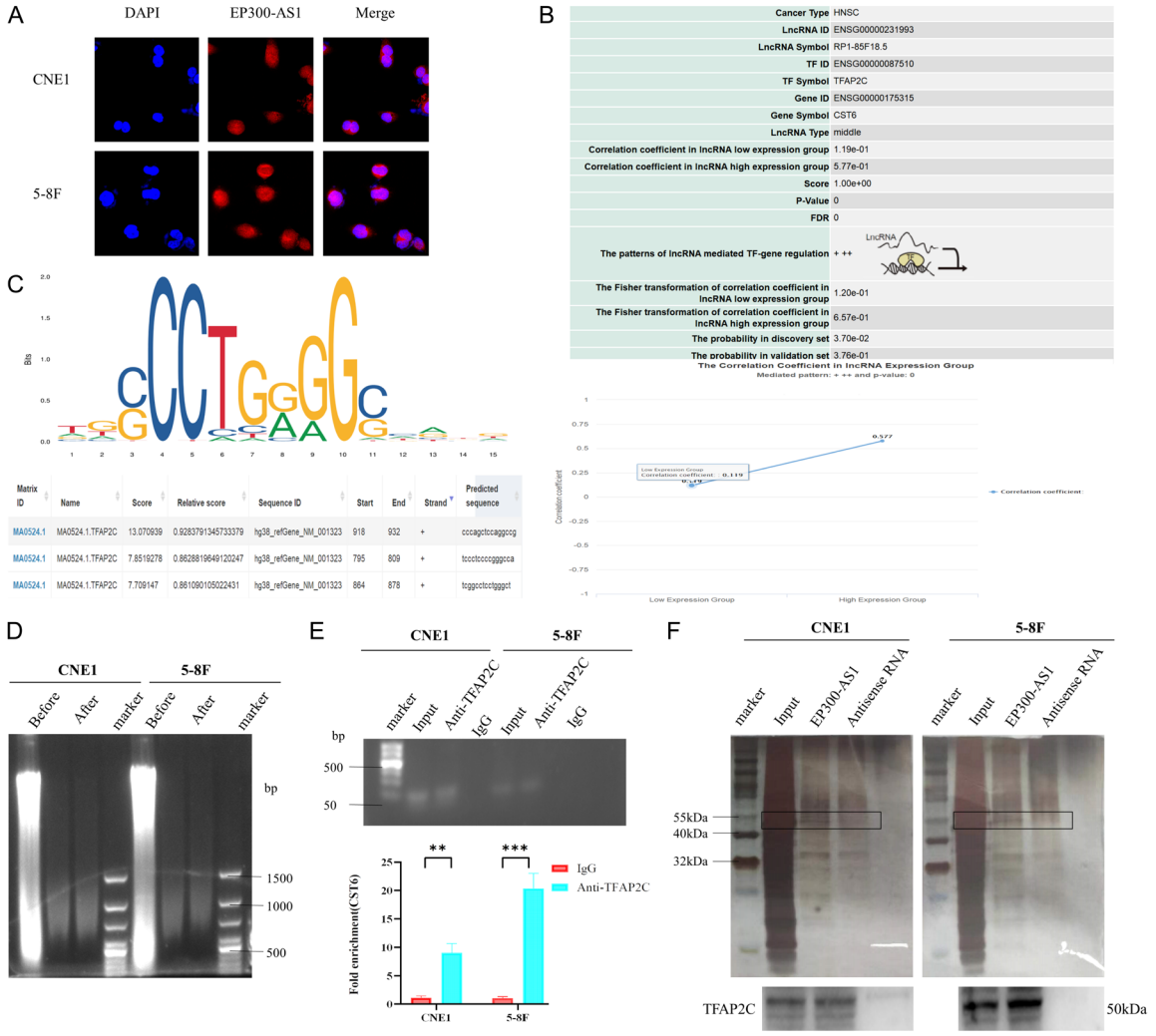

Figure 5. LncRNA EP300-AS1 Induces CST6 Expression via TFAP2C. A. FISH-based representative images illustrate the subcellular localization of lncRNA EP300-AS1 in CNE1 and 5-8F cells. B. The comprehensive findings for the lncRNA-TF-gene triplet, including the correlation coefficient for the lncRNA EP300-AS1 Expression Group, are compiled in the detailed information table sourced from the lncMAP database. C. The JASPAR database provides predicted binding motif site sequences for lncRNA EP300-AS1 and TFAP2C. D. DNA from NPC cell lines before and after ultrasound fragmentation. E. ChiP-PCR experiments reveal a relative increase in CST6 expression in the Anti-TFAP2C group compared to the IgG group, as corroborated by gel imaging of PCR products. F. Binding of lncRNA EP300-AS1 and TFAP2C is identified via silver staining and immunoblotting of RNA pull-down products. Scale bars = 20 μm.

tiple tissue types and demonstrate significant conservation [29].

lncRNA EP300-AS1 interaction with TFAP2C in HNSC: In head and neck squamous cell carcinoma (HNSC), we observed that lncRNA EP300-AS1 specifically targets CST6 by binding to the transcription factor TFAP2C. This interaction positively correlates with increased expression levels of lncRNA EP300-AS1, resulting in elevated CST6 levels bound to TFAP2C, as demonstrated in **Figure 5B**.

Transcription factor binding site analysis: Using the JASPAR CORE database, a resource with experimentally defined transcription factor binding sites for eukaryotes [30], we identified that lncRNA EP300-AS1, transcribed from the right-hand strand, possesses three TFAP2C binding sites (**Figure 5C**). This insight is crucial for understanding the transcriptional regulation mechanism of CST6.

Chromatin immunoprecipitation and PCR validation: We fragmented the nucleic acids of NPC cell lines using ultrasound, achieving fragments of approximately 1000 base pairs (**Figure 5D**). Subsequent chromatin immunoprecipitation followed by PCR (ChIP-PCR) revealed a significant increase in CST6 bound in both the Input group and the Anti-TFAP2C group compared to the IgG control, confirming TFAP2C's targeting of CST6 (**Figure 5E**).

Confirmation of lncRNA EP300-AS1 binding to TFAP2C: To confirm the direct interaction between EP300-AS1 and TFAP2C, we performed RNA pull-down and silver staining experiments. We first synthesized biotin-labeled EP300-AS1 RNA probes via in vitro transcription and incubated them with nasopha-ryngeal carcinoma (NPC) cell lysates in a buffer containing RNase inhibitors to facili-tate the formation of RNA-protein complexes. These complexes were then captured us-ing streptavidin magnetic beads, with multiple washes to remove non-specifically bound proteins. The captured proteins were separated by SDS-PAGE and analyzed for TFAP2C presence using Western blotting. A distinct TFAP2C band was observed in the EP300-AS1 probe group but not in the antisense negative control group (**Figure 5F**), confirming the direct interaction between EP300-AS1 and TFAP2C.

To further explore the composition of the RNA-protein complexes, we performed silver staining on the SDS-PAGE gels. The silver staining revealed several protein bands present exclusively in the EP300-AS1 probe group, absent in the antisense con-trol group (**Figure 5F**). The higher intensity of these bands in the EP300-AS1 probe group supports the specific binding of additional proteins to EP300-AS1, providing further evidence of the interaction between EP300-AS1 and TFAP2C.

Our research elucidates the regulatory role of lncRNA EP300-AS1 in NPC growth. It achieves this by activating CST6 expression through targeting the transcription fac-tor TFAP2C, thereby influencing critical gene regulatory pathways in nasopharyngeal carcinoma.

Investigating CST6 downregulation in nasopharyngeal carcinoma

Comparative tissue analysis: Our investigation commenced with a comparative examination involving 20 nasopharyngeal tissue specimens, evenly distributed between individuals without any pathology and those afflicted with carcinoma. The carcinoma-afflicted tissues exhibited distinct lymphoproliferative and hyperplastic fibrous characteristics, marked by cellular heterogeneity, short spindle-shaped nuclei displaying significant vesicular alterations, prominent nucleoli, as well as evident nuclear fission and necrosis (**Figure 6A**).

Immunohistochemical and immunofluorescent evidence of CST6 expression: Through immunohistochemical and immunofluorescent analyses, we made noteworthy observations. These analyses unveiled a significant decrease in CST6 expression within NPC tissues in comparison to their healthy counterparts (**Figure 6B**, **6C**). Furthermore, this consistent pattern of reduced CST6 expression was reflected in the NPC datasets from studies GSE12452 and GSE64634 (**Figure 6D**, **6E**).

Protein expression and database correlation: Upon extending our analysis to protein levels, with reference to the UNCLAN database, a consistent trend of decreased CST6 expression was noted in head and neck squamous cell carcinoma (**Figure 6F**).

Cellular level CST6 mRNA and protein expression: Subsequent cellular assays further validated our observations. Both mRNA and protein expression levels of CST6 were notably diminished in NPC cells relative to healthy nasopharyngeal cells (**Figure 6G**, **6H**).

The amalgamated data implies a potential tumor-suppressing function for CST6 in NPC. The observed downregulation of CST6 in NPC tissues and cell lines could offer crucial insights into the pathogenesis and progression of nasopharyngeal carcinoma.

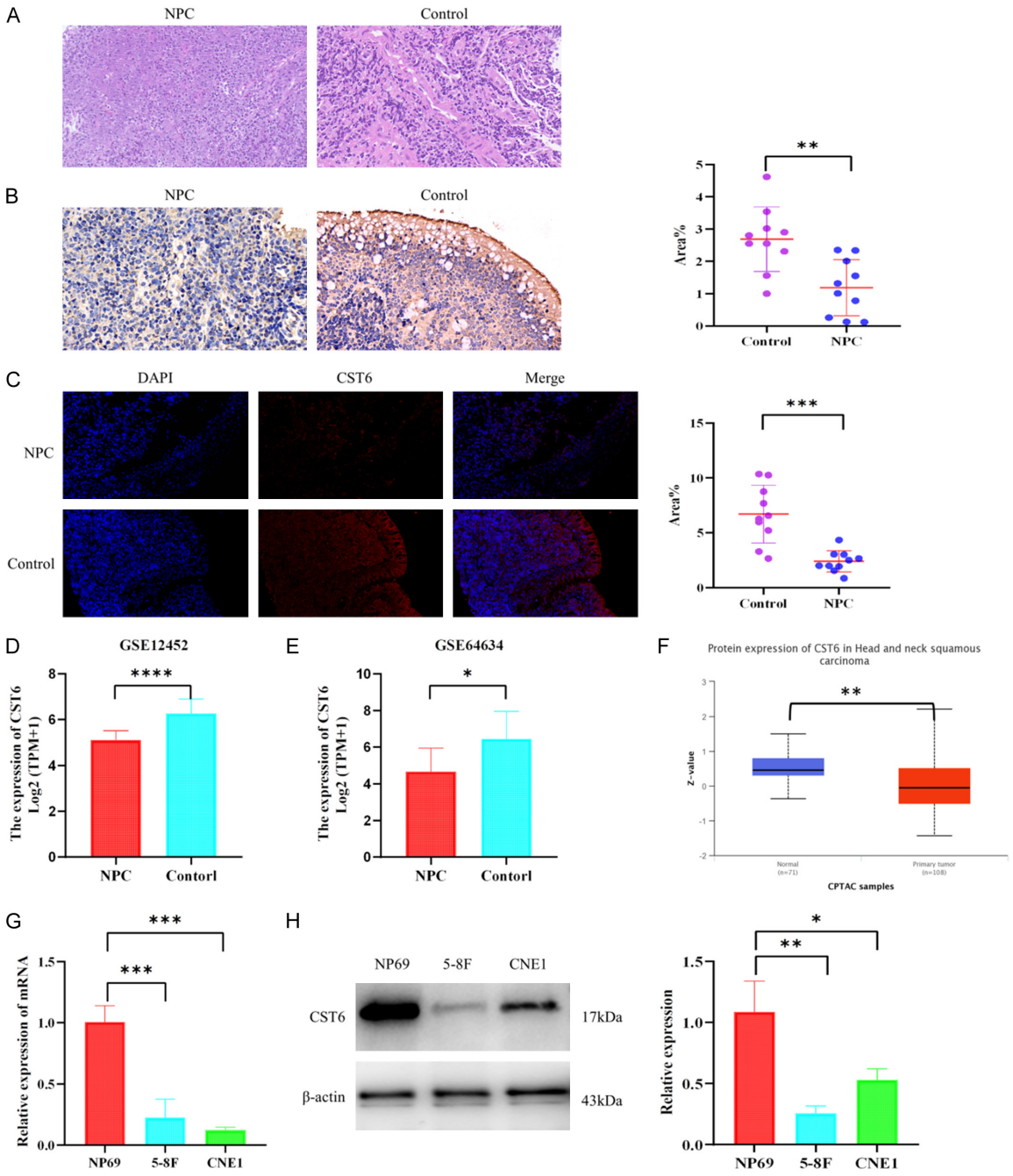

Figure 6. CST6 expression examination. A. Hematoxylin and eosin (H&E) staining of 10 pairs of human normal nasopharyngeal tissues and NPC tissues. B, C. Illustrative images from immunohistochemistry and immunofluorescence analyses detailing CST6 protein expression levels. D, E. CST6 expression as sequenced in the GSE12452 and GSE64634 datasets. F. Protein expression levels of CST6 in HNSC as derived from the UNCLAN database. G. Comparison of CST6 mRNA expression in NPC cell lines (CNE1 and 5-8F) versus normal nasopharyngeal cell lines (NP69). H. Comparative analysis of CST6 protein expression in NPC cell lines (CNE1 and 5-8F) and normal nasopharyngeal cell lines (NP69). Scale bars = 100 μm.

The role of CST6 as a tumor-suppressor factor in NPC

Exploring CST6 function in NPC: In our quest to unravel CST6's role in NPC, we devised an overexpression plasmid for CST6 and introduced it into NPC cells to establish stable expression (Figure S3A-D). This endeavor revealed that CST6 overexpression hampers the proliferation of NPC cells, as demonstrated

by both CCK8 and EdU incorporation assays (**Figure 7A-C**).

Further investigations: Expanding our inquiry, we utilized the transwell assay, colony formation experiment, and wound healing assay to investigate whether CST6 affects NPC cell motility, clonogenicity, and invasiveness. The outcomes suggests that the overexpression of CST6 remarkably inhibited the invasiveness, clonogenic potential, and migratory capabilities of NPC cells (Figure S4A-D).

Apoptosis analysis: Subsequently, we conducted an apoptosis assay, which revealed that CST6 overexpression accelerated the apoptosis of NPC cells (**Figure 7D**). Consistently, we noted an increase in the expression of pro-apoptotic proteins Bax and Caspases, accompanied by a decrease in the expression of the anti-apoptotic protein Bcl-2 (**Figure 7E**).

Cell cycle regulation: Ultimately, analysis of the cell cycle revealed that CST6 overexpression resulted in elevated expression levels of regulatory proteins Cyclin D1, CDK4, and CDK6 associated with the G0/G1 phase. Concurrently, there was a decrease in S-phase cells, with more NPC cells arrested in the G0/G1 phase (**Figure 7F**, **7G**).

Our findings indicate that CST6, regulated by lncRNA EP300-AS1, suppresses NPC cell proliferation, migration, clonogenicity, invasion, and promotes apoptosis.

CST6 controls EMT and restrains the development of NPC

CST6 expression and inhibition of xenograft growth: Our investigation into CST6's role in NPC involved subcutaneously implanting NPC cell lines CNE1 and 5-8F, engineered to stably overexpress CST6, into nude mice. Results depicted in **Figure 8A-C** demonstrate that CST6 overexpression significantly impeded xenograft tumor growth, highlighting its potential as a therapeutic target.

Relationship between CST6 levels and tumor progression: Further analysis revealed a negative correlation between increased CST6 expression in tumors and tumor growth, providing compelling evidence of CST6's inhibitory effects on tumor development (**Figure 8D**). This discovery was pivotal in delineating CST6's role in cancer biology.

CST6's influence on EMT marker expression: Subsequent investigations evaluated CST6's impact on EMT markers. The results showed that CST6 increased the expression of E-cadherin while decreasing the expression of N-cadherin, Vimentin, and Snail, providing evidence for its involvement in regulating EMT in both cellular and animal models.

Suppression of metastasis through EMT regulation: Taken together, these results suggest that CST6, potentially regulated by lncRNA EP300-AS1, can hinder distant metastasis and constrain NPC spread by regulating EMT processes, as depicted in **Figure 8E**, **8F**.

The interplay between methylation and immune cell regulation in NPC

Immune cell dynamics and NPC: Our study delved into the impact of immune cells on NPC, aiming to comprehend the interactions among B cells, CD4+ T cells, CD8+ T cells, macrophages, dendritic cells, and neutrophils alongside key molecular factors: CST6, TFAP2C, and lncRNA EP300-AS1. Our findings emphasized the notable involvement of macrophages in NPC, as illustrated in **Figure 9A-C**.

Epigenetic modifications and tumor microenvironment: Epigenetic processes, such as DNA methylation and modifications to histones, are pivotal in governing gene function. Methylation occurring on CpG islands within DNA promoter regions is a hallmark of early cancer development [31], influencing the advancement of tumors. These epigenetic changes also influence the immune microenvironment, allowing various immune cells to selectively affect cancer cells [32].

CST6 expression and methylation patterns: Typically, there exists an inverse relationship between gene expression and promoter methylation. Our analysis of the TCGA-HNSC methylation dataset identified specific loci - cg02349785, cg09482611, and cg14240536 - where methylation suppresses CST6 expression (**Figure 9D**). Further exploration through the MethSurv database revealed that methylation at cg09482611 correlates notably with patient prognosis, as shown in **Figure 9E**, **9F**.

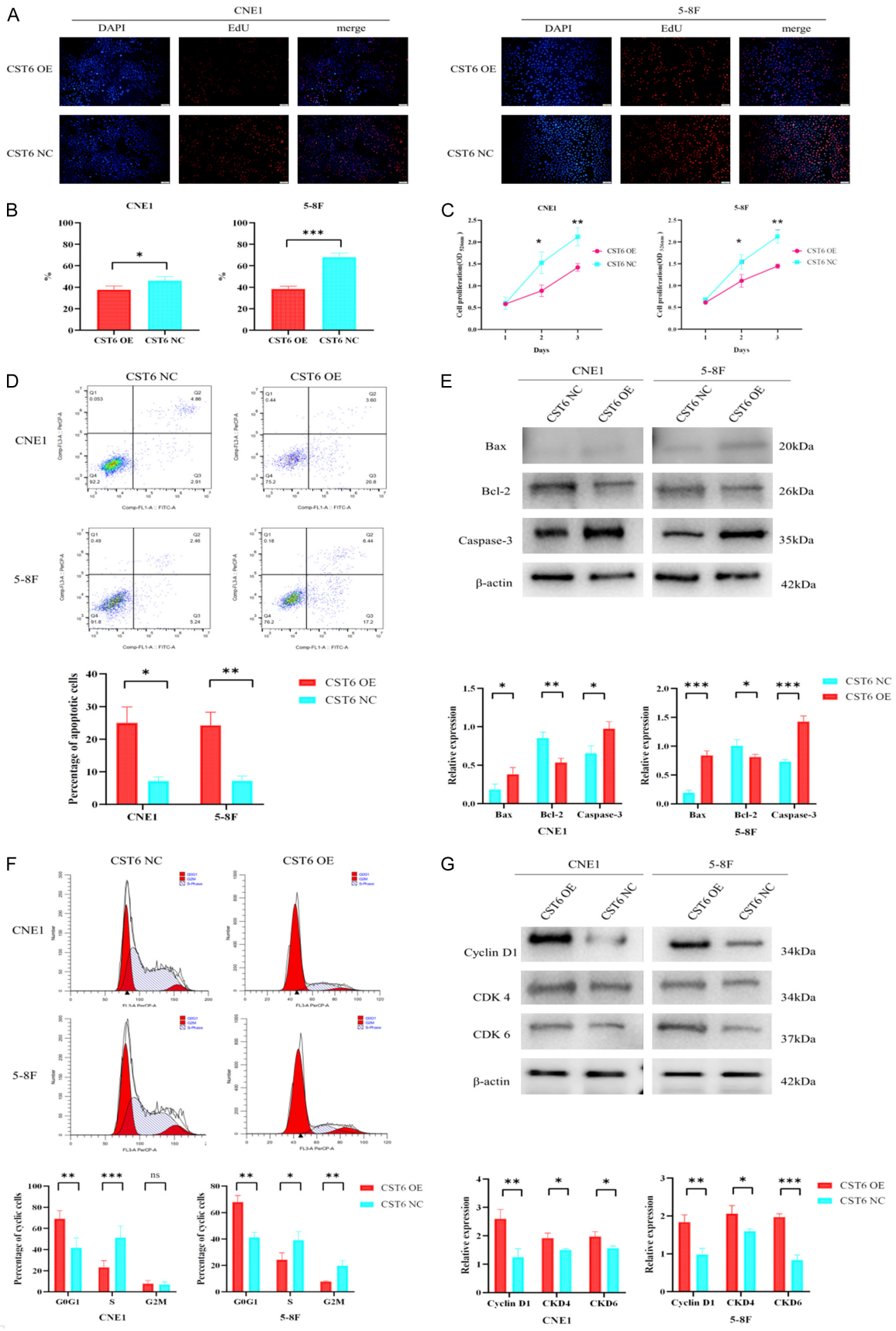
A
CNE1
5-8F
DAPI
EdU
merge
CST6 OE
CST6 NC
B
CNE1
5-8F
%
CST6 OE
CST6 NC
C
CNE1
5-8F
Cell proliferation(OD 52nm)
Days
CST6 OE
CST6 NC
D
CST6 NC
CST6 OE
CNE1
5-8F
Percentage of apoptotic cells
E
CNE1
5-8F
CST6 NC
CST6 OE
Bax
Bcl-2
Caspase-3
β-actin
20kDa
26kDa
35kDa
42kDa
Relative expression
F
CST6 NC
CST6 OE
CNE1
5-8F
Percentage of cyclic cells
G0G1
S
G2M
ns
G
CNE1
5-8F
Cyclin D1
CDK 4
CDK 6
34kDa
34kDa
37kDa
42kDa
CKD4
CKD6

Figure 7. CST6 inhibits proliferation, migration, clonality, and invasion of NPC cell lines. Cells from the CNE1 and 5-8F lines were transfected with pEGFP-C1 and pEGFP-C1-CST6. A, B. EdU incorporation assays were conducted to evaluate cell proliferation in control NPC cells and in those overexpressing CST6. Proliferating cells and EdU-positive nuclei are marked in red. C. Cell proliferation in both control and CST6-overexpressing NPC cells was assessed using CCK8 assays, with OD values at 450 nm indicating proliferation rates. D. CST6 overexpression induces apoptosis in NPC cells. E. Changes in the expression of apoptotic genes (Bax, Bcl-2, and Caspase-3) due to CST6 overexpression are presented. F. CST6 overexpression leads to alterations in NPC cell cycle distribution.The red tall regions represent the G0/G1 phase, while the low flat regions represent the G2/M phase. G. CST6 overexpression results in elevated expression of G0/G1 phase-related proteins: Cyclin D1, CDK4, and CDK6. Scale bars = 100 μm.

Regulatory role of methylation: Methylation Specific PCR (MSP) confirmed that CST6 expression in NPC is indeed regulated by promoter methylation, particularly in the CNE1 and 5-8F cell lines (**Figure 9G**). Moreover, a close association was observed between CST6 and lncRNA EP300-AS1 with various methylation-related genes, suggesting a shared regulatory mechanism for both CST6 and lncRNA EP300-AS1 (**Figure 9H**, **9I**).

Overall, our findings position CST6 and lncRNA EP300-AS1 as potential regulators of macrophage function and development through methylation pathways. These results lay the groundwork for further investigations to validate these regulatory pathways and their implications in NPC pathogenesis.

Discussion

Despite advances in radiation technology, the 5-year survival rate of NPC patients has not seen a significant increase, highlighting the urgent need to enhance the therapeutic impact of NPC. Efforts to address this should include early diagnosis and the identification of new therapeutic targets. Many studies have shown alterations in the expression of lncRNAs in NPC, some of which significantly regulate NPC development [33]. Our current work focused on the possible pathways by which lncRNA EP300-AS1 may affect the biological behavior of NPC cells.

Our study found that lncRNA EP300-AS1 activates TFAP2C to regulate CST6, thereby suppressing the malignant behavior of NPC cells and the EMT process. This research provides new theoretical foundations for clinical applications.

Due to the aggressive invasion and high metastasis inherent to NPC's biological traits, it poses substantial therapeutic challenges [34]. Preventing metastasis is key to improving prognosis and extending patient survival time. Studies have demonstrated the control of lncRNAs over various cancers, including NPC [35-37]. However, little is known about lncRNA EP300-AS1, which has been found to play a significant role in the proliferation, invasion, cell cycle, apoptosis, and cell scorching of rectal cancer cells [19]. In this study, we delve into the role of lncRNA EP300-AS1 in NPC, confirming its low expression in NPC and establishing its diagnostic value, making it a potentially useful biomarker.

Prior research has found several lncRNAs that significantly impact the prognosis of NPC, emphasizing the importance of prognostic molecular influences on cancer [38, 39]. We examined the survival of EP300-AS1 in HNSC and demonstrated, using univariate and multivariate COX analysis, that lncRNA EP300-AS1 was a distinct risk factor for HNSC prognosis. High expression of this lncRNA increased survival likelihood in OS, PFI, DSS, and DFS.

Some lncRNAs have recently been shown to affect the onset and progression of cancer through regulatory mechanisms in NPC. Discovering the regulatory mechanisms of particular lncRNAs in NPC is critical for identifying potential new therapeutic targets. We examined the subcellular location of lncRNA EP300-AS1 in NPC and found it to be primarily present in the nucleus. This suggests it may play a role in the nuclear route of NPC's malignant biological behavior. Furthermore, we verified the interaction between lncRNA EP300-AS1, TFAP2, and CST6 and found that lncRNA EP300-AS1 positively controls CST6 gene expression through TFAP2C, thereby suppressing NPC cell proliferation, cell cycle progression, migration, invasion, and clone formation while promoting apoptosis.

CST6 has been shown in previous studies to inhibit EMT in HNSC [18], which contributes to

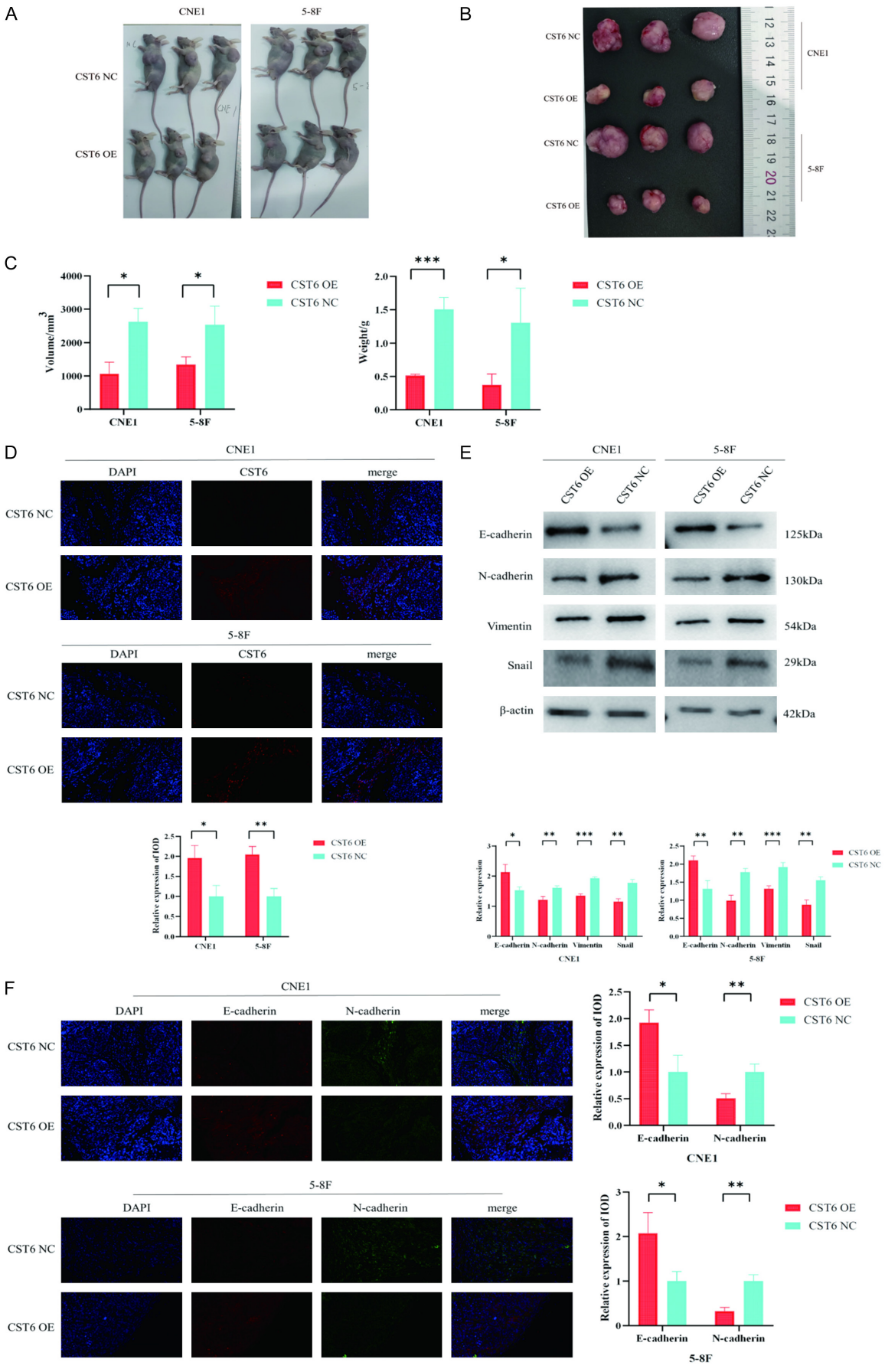
A
CNE1
5-8F
CST6 NC
CST6 OE
B
CST6 NC
CST6 OE
CST6 NC
CST6 OE
CNE1
5-8F
C
Volume/mm3
CST6 OE
CST6 NC
CNE1
5-8F
Weight/g
CST6 OE
CST6 NC
CNE1
5-8F
D
CNE1
DAPI
CST6
merge
CST6 NC
CST6 OE
5-8F
DAPI
CST6
merge
CST6 NC
CST6 OE
Relative expression of IOD
CST6 OE
CST6 NC
CNE1
5-8F
E
CNE1
5-8F
CST6 OE
CST6 NC
CST6 OE
CST6 NC
E-cadherin
N-cadherin
Vimentin
Snail
β-actin
125kDa
130kDa
54kDa
29kDa
42kDa
Relative expression
E-cadherin
N-cadherin
Vimentin
Snail
CNE1
5-8F
CST6 OE
CST6 NC
F
CNE1
DAPI
E-cadherin
N-cadherin
merge
CST6 NC
CST6 OE
5-8F
DAPI
E-cadherin
N-cadherin
merge
CST6 NC
CST6 OE
Relative expression of IOD
E-cadherin
N-cadherin
CNE1
5-8F
CST6 OE
CST6 NC

Figure 8. CST6 Modulates NPC Growth and EMT Processes. A, B. Images before and after tumor excision in nude mice, 28 days post tumor induction. C. On day 28 post-inoculation, mice were euthanized, tumors were excised, and their volumes were determined. The mice's weights were also recorded. D. CST6 expression in nude mice post tumor induction. E. In CNE1 and 5-8F cell lines, CST6 overexpression elevates E-cadherin levels and diminishes N-cadherin, Vimentin, and Snail expression. F. During tumorigenesis in nude mice, CST6 influences the expression of EMT markers, including E-cadherin, N-cadherin, Vimentin, and Snail. Scale bars = 100 μm.

cancer metastasis and relapse [40]. Our experiments, conducted both in vivo and in vitro, illustrated that elevated expression of CST6 in NPC cells led to an increase in E-cadherin expression and a decrease in N-cadherin expression. This suggests that lncRNA EP300-AS1 can prevent the development of EMT by interfering with CST6.

The emergence of immunotherapies, treatments that leverage the power of the immune system to fight cancer cells [41], has highlighted the importance of understanding how immune cells regulate NPC. This study revealed that the lncRNAs EP300-AS1, TFAP2C, and CST6 contribute to macrophage suppression. CST6 was regulated by methylation in NPC cell lines, while both lncRNA EP300-AS1 or CST6 were associated with multiple methylation gene regulations. We propose that lncRNA EP300-AS1 and CST6 may regulate macrophage progression through methylation, although further experiments are needed to validate this hypothesis.

Additionally, the lncRNA EP300-AS1 may regulate tumor progression through mechanisms involving microRNAs (miRNAs). One common mechanism is the competitive endogenous RNA (ceRNA) hypothesis, in which lncRNAs act as "sponges" that bind to miRNAs and reduce their ability to inhibit target mRNAs [42]. EP300-AS1 may also directly bind to miRNA precursors or mature miRNAs, thereby affecting their processing, stability, or activity [43]. Furthermore, EP300-AS1 can interact with protein complexes that influence miRNA biogenesis and function [42]. Collectively, these interactions modulate the expression of oncogenes and tumor suppressor genes, either promoting tumor cell proliferation, migration, and invasion or inhibiting tumor progression. Thus, both lncRNA EP300-AS1 and miRNAs represent promising biomarkers and potential targets for personalized cancer therapies.

Firstly, our study demonstrates that lncRNA EP300-AS1 regulates CST6 by activating TFAP2C, thereby inhibiting malignant behaviors and EMT in NPC cells. This finding provides a novel theoretical basis for clinical applications, particularly in developing new diagnostic markers and therapeutic targets. Given the highly invasive and metastatic nature of NPC, preventing metastasis is crucial for improving prognosis and extending patient survival. Consequently, therapies targeting EP300-AS1 may offer a promising strategy for controlling NPC progression. However, targeting EP300-AS1 presents several challenges. For instance, precisely regulating its expression without disrupting normal physiological processes remains a significant hurdle. Additionally, although our study indicates that low EP300-AS1 expression correlates with poor prognosis in NPC, further large-scale clinical trials are necessary to validate its efficacy as an independent prognostic factor. Future research should focus on elucidating the interactions among EP300-AS1, TFAP2C, and CST6, particularly whether these interactions vary across different NPC subtypes. Moreover, conducting more preclinical and clinical trials to assess the safety and efficacy of targeting these molecular pathways is essential. Considering genetic differences among individuals, developing personalized treatment strategies will be key to improving therapeutic outcomes.

We acknowledge several limitations in our study. First, the clinical sample size was relatively small, consisting of 10 NPC patients and 10 control subjects, which may limit the statistical power and generalizability of our findings. Future studies with larger sample sizes will be necessary to further validate these results. Second, while we used BALB/c nude mice to establish NPC xenograft models, these models might not fully capture the complexity of human NPC, particularly regarding the immune microenvironment. As such, the translational value of our results for human disease still re-quires further validation. Lastly, although our study provides novel insights into the diagnosis, prognosis, and treatment of NPC, the clinical applica-

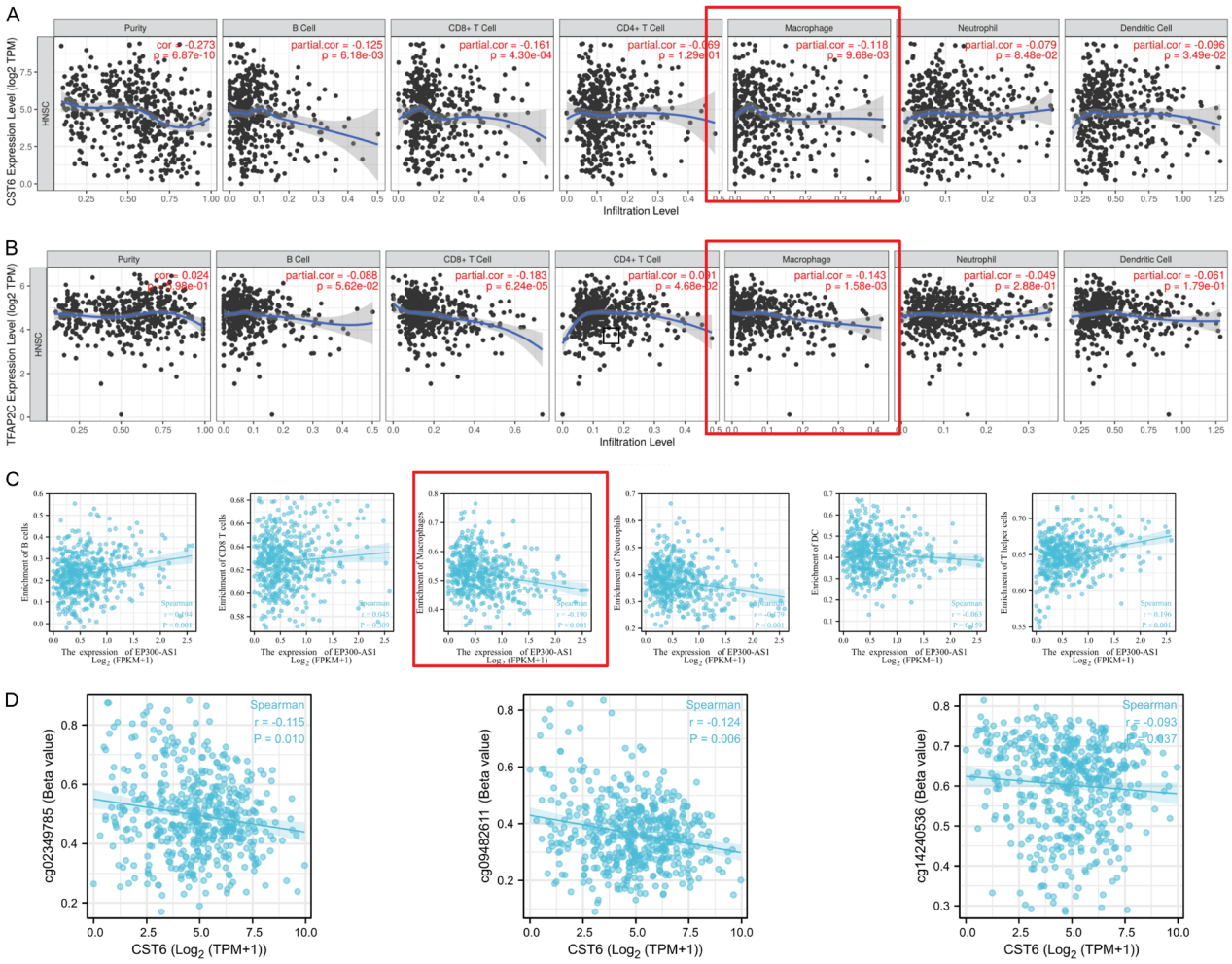
A
Purity
B Cell
CD8+ T Cell
CD4+ T Cell
Macrophage
Neutrophil
Dendritic Cell
CST6 Expression Level (log2 TPM)
HNSC
Infiltration Level
B
TFAP2C Expression Level (log2 TPM)
C
Enrichment of B cells
Enrichment of CD8 T cells
Enrichment of Macrophages
Enrichment of Neutrophils
Enrichment of DC
Enrichment of T helper cells
The expression of EP300-AS1 Log2 (FPKM+1)
D
cg02349785 (Beta value)
cg09482611 (Beta value)
cg14240536 (Beta value)
CST6 (Log2 (TPM+1))
Spearman
r = -0.115
P = 0.010
r = -0.124
P = 0.006
r = -0.093
P = 0.037

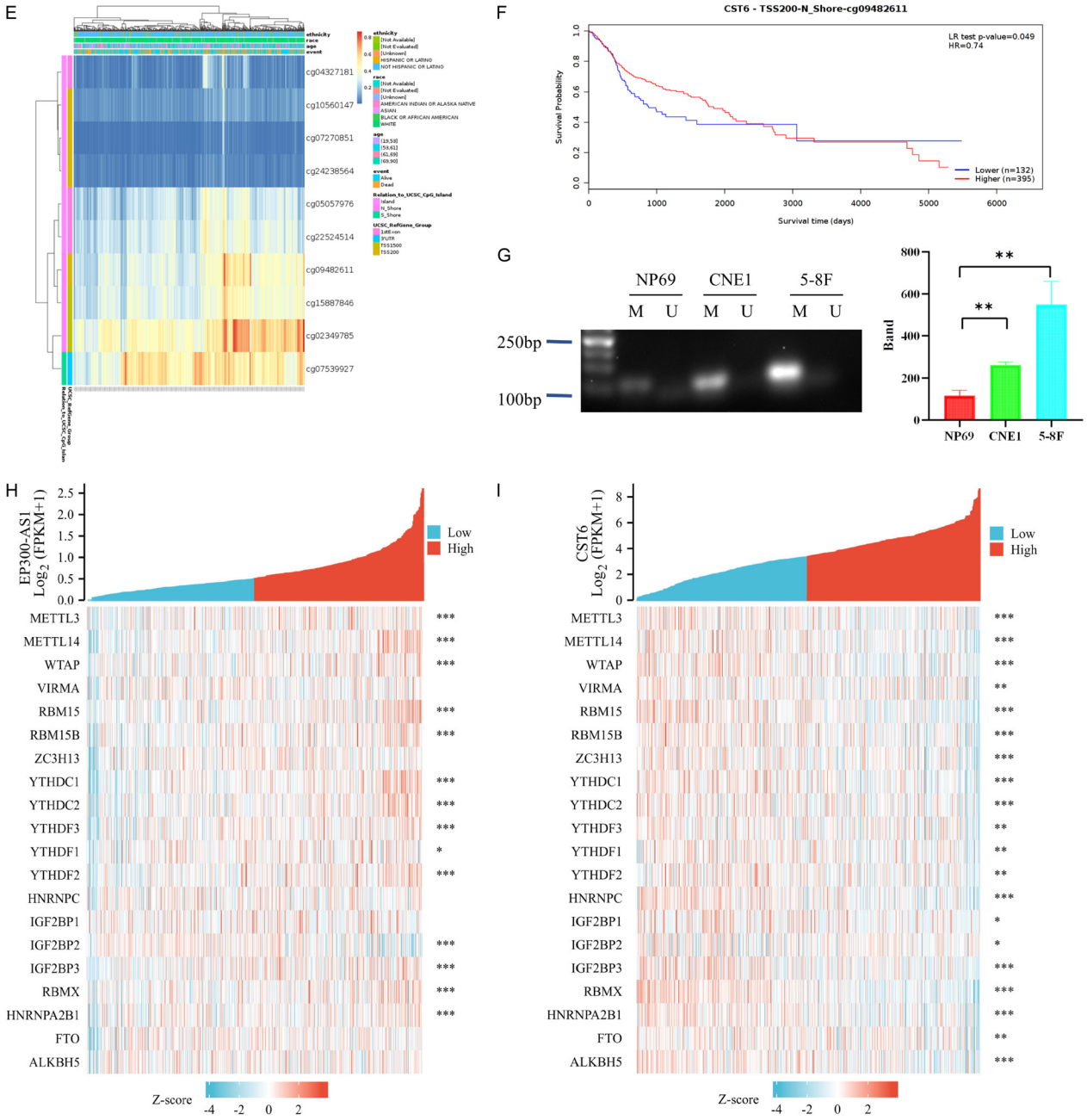
E
cg04327181
cg10560147
cg07270851
cg24238564
cg05057976
cg22524514
cg09482611
cg15887846
cg02349785
cg07539927
F
CST6 - TSS200-N_Shore-cg09482611
LR test p-value=0.049
HR=0.74
Survival Probability
Survival time (days)
Lower (n=132)
Higher (n=395)
G
NP69
CNE1
5-8F
M U M U M U
250bp
100bp
Band
NP69
CNE1
5-8F
H
EP300-AS1 Log2 (FPKM+1)
Low
High
METTL3
METTL14
WTAP
VIRMA
RBM15
RBM15B
ZC3H13
YTHDC1
YTHDC2
YTHDF3
YTHDF1
YTHDF2
HNRNPC
IGF2BP1
IGF2BP2
IGF2BP3
RBMX
HNRNPA2B1
FTO
ALKBH5
Z-score
I
CST6 Log2 (FPKM+1)
Low
High
Z-score

Figure 9. Methylation regulation and immune correlation analyses. (A, B) TIMER analysis of the correlation between CST6 (A) and TFAP2C (B) with immune cell types: B cells, CD4+ T cells, CD8+ T cells, macrophages, dendritic cells, and neutrophils. (C) TCGA analysis showing correlation between CST6 and the aforementioned immune cells. (D) Investigation of the correlation between methylation and CST6 at sites cg02349785, cg09482611, and cg14240536 within the TCGA-HNSC methylation dataset. (E) Heat map representation of CST6 expression in HNSC. (F) Survival analysis associated with the CpG site cg09482611 of CST6 in HNSC. (G) Methylation status of CST6 in NPC cells determined by MSP, with U indicating unmethylated and M representing methylated sequences. (H, I) Heat maps showcasing correlations between lncRNA EP300-AS1 (H) and CST6 (I) with methylation genes.

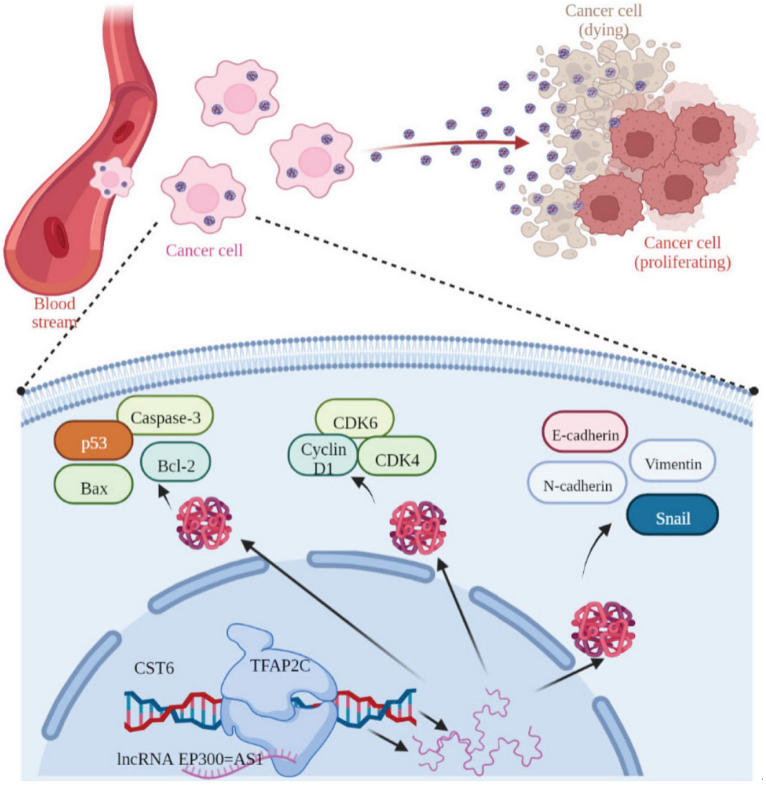

Figure 10. In NPC, the lncRNA EP300-AS1 plays a crucial role in tumor suppression by targeting the transcription factor TFAP2C, influencing its binding to the promoter region of CST6 and thereby regulating CST6 expression. This regulatory mechanism inhibits cancer cell proliferation by promoting apoptosis through the upregulation of pro-apoptotic proteins such as Bax and Caspase-3, while downregulating the anti-apoptotic protein Bcl-2. Additionally, EP300-AS1 modulates the cell cycle, arresting cancer cells in the G0/G1 phase, as evidenced by increased expression of key cell cycle regulators including Cyclin D1, CDK4, and CDK6. Furthermore, EP300-AS1 promotes the transition of cancer cells from a mesenchymal to an epithelial state by downregulating mesenchymal markers (vimentin, N-cadherin, Snail) and upregulating the epithelial marker E-cadherin, indicating a potential reversal of EMT. These combined effects highlight EP300-AS1's therapeutic potential in controlling tumor growth and metastasis in NPC.

bility of these findings will need to be confirmed through additional clinical trials to assess their safety and efficacy. We recognize these limitations as important directions for future research, and we plan to address them by increasing our sample size, improving experimental models, and conducting further clinical trials to enhance the robustness and clinical relevance of our study.

Conclusions

This research unveils that a novel lncRNA, EP300-AS1, experiences down-regulation in NPC. Overexpression of lncRNA EP300-AS1 in NPC cells significantly impedes the EMT process and disrupts various cellular functions including viability, proliferation, clone formation, cell cycle progression, invasion, and migration. Moreover, the tumor-forming ability of lncRNA EP300-AS1 is diminished in in vivo experiments.

Our investigation further indicates that the oncogenic effects of lncRNA EP300-AS1 may arise from its direct interaction with TFAP2C/CST6 (**Figure 10**). We propose that the modulation of macrophage transformation could be influenced by the interplay between lncRNA EP300-AS1, CST6, and methylation. In the context of NPC, EP300-AS1 targets the transcription factor TFAP2C, consequently leading to the upregulation of CST6, as depicted in **Figure 10**. Notably, the relationship between lncRNA EP300-AS1, TFAP2C, CST6, and various immune cells suggests a significant connection with macrophages. Additionally, there exists a negative correlation between DNA methylation levels and CST6 expression. Interestingly, methylation at specific loci within CST6 may have varying impacts on patient

prognosis. Future investigations should delve deeper into comprehending the regulatory influence of methylation in NPC.

Additionally, we further highlight the therapeutic significance of targeting EP300-AS1. Our findings demonstrate that EP300-AS1 exhibits tumor-suppressive activity in NPC by inhibiting cell proliferation, migration, and invasion, promoting apoptosis, and regulating the expression of EMT markers. These results suggest that EP300-AS1 could serve as both a promising therapeutic target and a potential biomarker for NPC. However, translating these insights into clinical practice poses several challenges, including the need to elucidate the precise mechanisms of action of EP300-AS1, confirm its safety and efficacy in human patients, and address tumor heterogeneity for personalized therapies.

Future research will focus on a deeper exploration of the interactions between EP300-AS1, TFAP2C, and CST6, conducting additional preclinical and clinical trials, and developing tailored treatment strategies for individual patients. This study not only advances the understanding of NPC pathogenesis but also opens new avenues for improving patient care and therapeutic outcomes through personalized approaches.

Acknowledgements

This work was supported by the Hainan graduate student innovation project (number: Qhyb2023-181) and the Natural Science Foundation of Hainan Province, China (number: 824QN381). The publication fees for this article were supported by the UNLV University Libraries Open Article Fund.

Disclosure of conflict of interest

None.

Abbreviations

HNSC, Head and neck squamous carcinoma; NPC, Nasopharyngeal carcinoma; LncRNA, Long non-coding RNA; EMT, Epithelial mesenchymal transition; CeRNAs, Competitive RNAs; AR, Androgen receptor; OS, Overall survival; PFI, Progression-free interval; DSS, Disease-specific survival.

Address correspondence to: Zhonglin Mu, Department of Otolaryngology, Head and Neck Surgery, The First Affiliated Hospital of Hainan Medical University, Haikou 570102, Hainan, China. E-mail: hy0101008@hainmc.edu.cn; Qibing Liu, Department of Pharmacy, The First Affiliated Hospital of Hainan Medical University, Haikou 570102, Hainan, China. E-mail: qibing.liu@hainmc.edu.cn; Yu Kuang, Medical Physics Program, University of Nevada, Las Vegas, Las Vegas, NV 89154, USA. E-mail: yu.kuang@unlv.edu

References

[1] Chen YP, Chan ATC, Le QT, Blanchard P, Sun Y and Ma J. Nasopharyngeal carcinoma. Lancet 2019; 394: 64-80.
[2] Wei WI and Sham JS. Nasopharyngeal carcinoma. Lancet 2005; 365: 2041-2054.
[3] Lee AW, Lin JC and Ng WT. Current management of nasopharyngeal cancer. Semin Radiat Oncol 2012; 22: 233-244.
[4] Lee AW, Ma BB, Ng WT and Chan AT. Management of nasopharyngeal carcinoma: current practice and future perspective. J Clin Oncol 2015; 33: 3356-3364.
[5] Genova P, Brunetti F, Bequignon E, Landi F, Lizzi V, Esposito F, Charpy C, Calderaro J, Azoulay D and de'Angelis N. Solitary splenic metastasis from nasopharyngeal carcinoma: a case report and systematic review of the literature. World J Surg Oncol 2016; 14: 184.
[6] Mercer TR, Dinger ME and Mattick JS. Long non-coding RNAs: insights into functions. Nat Rev Genet 2009; 10: 155-159.
[7] Gibb EA, Brown CJ and Lam WL. The functional role of long non-coding RNA in human carcinomas. Mol Cancer 2011; 10: 38.
[8] Chen SX, Yin JF, Lin BC, Su HF, Zheng Z, Xie CY and Fei ZH. Upregulated expression of long noncoding RNA SNHG15 promotes cell proliferation and invasion through regulates MMP2/MMP9 in patients with GC. Tumour Biol 2016; 37: 6801-6812.
[9] Zhang JH, Wei HW and Yang HG. Long noncoding RNA SNHG15, a potential prognostic biomarker for hepatocellular carcinoma. Eur Rev Med Pharmacol Sci 2016; 20: 1720-1724.
[10] Eckner R, Ewen ME, Newsome D, Gerdes M, DeCaprio JA, Lawrence JB and Livingston DM. Molecular cloning and functional analysis of the adenovirus E1A-associated 300-kD protein (p300) reveals a protein with properties of a transcriptional adaptor. Genes Dev 1994; 8: 869-884.
[11] Chen Z, Lei T, Chen X, Gu J, Huang J, Lu B and Wang Z. Long non-coding RNA in lung cancer. Clin Chim Acta 2020; 504: 190-200.

[12] Zhao H, Liu X, Yu L, Lin S, Zhang C, Xu H, Leng Z, Huang W, Lei J, Li T, Li J, Yang F and Wang L. Comprehensive landscape of epigenetic-dysregulated lncRNAs reveals a profound role of enhancers in carcinogenesis in BC subtypes. Mol Ther Nucleic Acids 2021; 23: 667-681.
[13] Gu R, Liu M, Lin P, Feng TY, Yuan H, Ou DQ, Li SQ, Li Q, Zhao G, Zhang J and Li K. Correlation analysis of poor prognosis and immunotherapy of lncRNAs related with m (6)A modification in cervical cancer. Sichuan Da Xue Xue Bao Yi Xue Ban 2022; 53: 626-636.
[14] Zeeuwen PL, Cheng T and Schalkwijk J. The biology of cystatin M/E and its cognate target proteases. J Invest Dermatol 2009; 129: 1327-1338.
[15] Sotiropoulou G, Anisowicz A and Sager R. Identification, cloning, and characterization of cystatin M, a novel cysteine proteinase inhibitor, down-regulated in breast cancer. J Biol Chem 1997; 272: 903-910.
[16] Shridhar R, Zhang J, Song J, Booth BA, Kevil CG, Sotiropoulou G, Sloane BF and Keppler D. Cystatin M suppresses the malignant phenotype of human MDA-MB-435S cells. Oncogene 2004; 23: 2206-2215.
[17] Veena MS, Lee G, Keppler D, Mendonca MS, Redpath JL, Stanbridge EJ, Wilczynski SP and Srivatsan ES. Inactivation of the cystatin E/M tumor suppressor gene in cervical cancer. Genes Chromosomes Cancer 2008; 47: 740-754.
[18] Xu D, Ding S, Cao M, Yu X, Wang H, Qiu D, Xu Z, Bi X, Mu Z and Li K. A pan-cancer analysis of cystatin E/M reveals its dual functional effects and positive regulation of epithelial cell in human tumors. Front Genet 2021; 12: 733211.
[19] Ma Y, Chen Y, Lin C and Hu G. Biological functions and clinical significance of the newly identified long non-coding RNA RP1-85F18.6 in colorectal cancer. Oncol Rep 2018; 40: 2648-2658.
[20] Song J, Song W and Zhang L. LncRNA RP1-85F18.6 affects osteoblast cells by regulating the cell cycle. Open Life Sci 2020; 15: 951-958.
[21] Mo Y, Wang Y, Xiong F, Ge X, Li Z, Li X, Li Y, Li X, Xiong W, Li G, Zeng Z and Guo C. Proteomic analysis of the molecular mechanism of lovastatin inhibiting the growth of nasopharyngeal carcinoma cells. J Cancer 2019; 10: 2342-2349.
[22] Liao LJ, Hsu WL, Chen CJ and Chiu YL. Feature reviews of the molecular mechanisms of nasopharyngeal carcinoma. Biomedicines 2023; 11: 1528.
[23] Xin Z, Hu C, Zhang C, Liu M, Li J, Sun X, Hu Y, Liu X and Wang K. LncRNA-HMG incites colorectal cancer cells to chemoresistance via repressing p53-mediated ferroptosis. Redox Biol 2024; 77: 103362.
[24] Li WH, Dang Y, Zhang L, Zhou JC, Zhai HY, Yang Z, Ma K and Wang ZZ. METTL3-mediated m(6)A methylation of DNMT1 promotes the progression of non-small cell lung cancer by regulating the DNA methylation of FOXO3a. Heliyon 2024; 10: e28618.
[25] Wang L, Zhang X, Lin ZB, Yang PJ, Xu H, Duan JL, Ruan B, Song P, Liu JJ, Yue ZS, Fang ZQ, Hu H, Liu Z, Huang XL, Yang L, Tian S, Tao KS, Han H and Dou KF. Tripartite motif 16 ameliorates nonalcoholic steatohepatitis by promoting the degradation of phospho-TAK1. Cell Metab 2021; 33: 1372-1388.e1377.
[26] Li J, Varghese RS and Ressom HW. RNA-seq data analysis. Methods Mol Biol 2024; 2822: 263-290.
[27] Wang WT, Chen TQ, Zeng ZC, Pan Q, Huang W, Han C, Fang K, Sun LY, Yang QQ, Wang D, Luo XQ, Sun YM and Chen YQ. The lncRNA LAMP5-AS1 drives leukemia cell stemness by directly modulating DOT1L methyltransferase activity in MLL leukemia. J Hematol Oncol 2020; 13: 78.
[28] Obuchowski NA and Bullen JA. Receiver operating characteristic (ROC) curves: review of methods with applications in diagnostic medicine. Phys Med Biol 2018; 63: 07TR01.
[29] Li Y, Li L, Wang Z, Pan T, Sahni N, Jin X, Wang G, Li J, Zheng X, Zhang Y, Xu J, Yi S and Li X. LncMAP: pan-cancer atlas of long noncoding RNA-mediated transcriptional network perturbations. Nucleic Acids Res 2018; 46: 1113-1123.
[30] Castro-Mondragon JA, Riudavets-Puig R, Rauluseviciute I, Lemma RB, Turchi L, Blanc-Mathieu R, Lucas J, Boddie P, Khan A, Manosalva Pérez N, Fornes O, Leung TY, Aguirre A, Hammal F, Schmelter D, Baranasic D, Ballester B, Sandelin A, Lenhard B, Vandepoele K, Wasserman WW, Parcy F and Mathelier A. JASPAR 2022: the 9th release of the open-access database of transcription factor binding profiles. Nucleic Acids Res 2022; 50: D165-D173.
[31] Li D, Zhang L, Liu Y, Sun H, Onwuka JU, Zhao Z, Tian W, Xu J, Zhao Y and Xu H. Specific DNA methylation markers in the diagnosis and prognosis of esophageal cancer. Aging (Albany NY) 2019; 11: 11640-11658.
[32] Zhang B, Wu Q, Li B, Wang D, Wang L and Zhou YL. m(6)A regulator-mediated methylation modification patterns and tumor microenvironment infiltration characterization in gastric cancer. Mol Cancer 2020; 19: 53.
[33] Wang H, Wang W and Fan S. Emerging roles of lncRNA in nasopharyngeal carcinoma and

therapeutic opportunities. Int J Biol Sci 2022; 18: 2714-2728.
[34] Lin M, Zhang XL, You R, Yang Q, Zou X, Yu K, Liu YP, Zou RH, Hua YJ, Huang PY, Wang J, Zhao Q, Jiang XB, Tang J, Gu YK, Yu T, He GP, Xie YL, Wang ZQ, Liu T, Chen SY, Zuo ZX and Chen MY. Neoantigen landscape in metastatic nasopharyngeal carcinoma. Theranostics 2021; 11: 6427-6444.
[35] Li ZX, Zheng ZQ, Yang PY, Lin L, Zhou GQ, Lv JW, Zhang LL, Chen F, Li YQ, Wu CF, Li F, Ma J, Liu N and Sun Y. WTAP-mediated m(6)A modification of lncRNA DIAPH1-AS1 enhances its stability to facilitate nasopharyngeal carcinoma growth and metastasis. Cell Death Differ 2022; 29: 1137-1151.
[36] Zhou L, Liu R, Liang X, Zhang S, Bi W, Yang M, He Y, Jin J, Li S, Yang X, Fu J and Zhang P. lncRNA RP11-624L4.1 is associated with unfavorable prognosis and promotes proliferation via the CDK4/6-cyclin D1-Rb-E2F1 pathway in NPC. Mol Ther Nucleic Acids 2020; 22: 1025-1039.
[37] Zheng ZQ, Li ZX, Zhou GQ, Lin L, Zhang LL, Lv JW, Huang XD, Liu RQ, Chen F, He XJ, Kou J, Zhang J, Wen X, Li YQ, Ma J, Liu N and Sun Y. Long noncoding RNA FAM225A promotes nasopharyngeal carcinoma tumorigenesis and metastasis by acting as ceRNA to sponge miR-590-3p/miR-1275 and upregulate ITGB3. Cancer Res 2019; 79: 4612-4626.
[38] Yang X, Lin F and Gao F. Up-regulated long noncoding RNA ILF3-AS1 indicates poor prognosis of nasopharyngeal carcinoma and promoted cell metastasis. Int J Biol Markers 2020; 35: 61-70.
[39] Yao L, Wang T and Wang X. LncRNA FOXP4-AS1 serves as a biomarker for nasopharyngeal carcinoma diagnosis and prognosis. 3 Biotech 2021; 11: 25.
[40] Zhang Y and Weinberg RA. Epithelial-to-mesenchymal transition in cancer: complexity and opportunities. Front Med 2018; 12: 361-373.
[41] Rosenberg SA. Cancer immunotherapy comes of age. Nat Clin Pract Oncol 2005; 2: 115.
[42] Ma B, Wang S, Wu W, Shan P, Chen Y, Meng J, Xing L, Yun J, Hao L, Wang X, Li S and Guo Y. Mechanisms of circRNA/lncRNA-miRNA interactions and applications in disease and drug research. Biomed Pharmacother 2023; 162: 114672.
[43] Paraskevopoulou MD and Hatzigeorgiou AG. Analyzing MiRNA-LncRNA interactions. Methods Mol Biol 2016; 1402: 271-286.

Table S1. 100 genes most associated with lncRNA EP300-AS1 in HNSC

Gene_name	Cor_pearson	P_pearson
C5orf66	0.600594596	1.57E-50
HLF	0.593386005	4.50E-49
PDIK1L	0.590400996	1.76E-48
LRRC8B	0.582056219	7.42E-47
CYB5RL	0.569302939	1.84E-44
MT2A	-0.560469895	7.29E-43
MEIS1	0.558982339	1.34E-42
KLB	0.553872193	1.06E-41
TXNDC16	0.545055075	3.46E-40
ZNF541	0.544107419	5.01E-40
C15orf41	0.542931652	7.90E-40
NCK1	0.542381967	9.76E-40
EPHX3	0.540232264	2.23E-39
TET2	0.538772469	3.90E-39
FOXRED2	0.535409771	1.40E-38
FBXO34	0.535272259	1.47E-38
AC008406.3	0.53505564	1.60E-38
LIN54	0.532678565	3.89E-38
MYO5C	0.532471054	4.21E-38
MTMR1	0.532218716	4.62E-38
FSTL3	-0.532028175	4.96E-38
RELCH	0.531824267	5.36E-38
FAM3B	0.530304387	9.42E-38
PIGN	0.530163948	9.92E-38
SCYL3	0.529479979	1.28E-37
MIR9-3HG	0.528344395	1.94E-37
EPB41L4A	0.527730489	2.44E-37
RAB11FIP1	0.527204758	2.96E-37
SCAI	0.526659459	3.61E-37
PRDM15	0.526186635	4.29E-37
BICDL1	0.524577946	7.72E-37
GLS2	0.524019454	9.45E-37
FOXA1	0.522494622	1.64E-36
CENPC	0.522316871	1.75E-36
IKZF2	0.522084459	1.90E-36
RPS6KA5	0.52207528	1.91E-36
CBFA2T2	0.521282325	2.54E-36
ILDR1	0.520883749	2.93E-36
RAD9B	0.520634708	3.21E-36
AC007191.1	0.517963511	8.34E-36
ATAD2B	0.51765586	9.30E-36
TESK2	0.517592509	9.51E-36
ACAP2	0.517349176	1.04E-35
E2F2	0.517254246	1.07E-35
OGFRL1	0.516801756	1.26E-35
SLC25A40	0.516505639	1.40E-35
ZNF396	0.5150454	2.34E-35
FAM83E	0.514951171	2.42E-35
GRHL3-AS1	0.514874251	2.49E-35

LRRC37A14P	0.514679736	2.66E-35
KLF3	0.514495638	2.84E-35
PPM1D	0.514030226	3.35E-35
DTX2P1-UPK3BP1-PMS2P11	0.513600194	3.89E-35
MAGI3	0.513332474	4.28E-35
ZYG11A	0.512585778	5.55E-35
MBNL3	0.511745814	7.45E-35
SOX21-AS1	0.510690752	1.08E-34
BARD1	0.510154754	1.29E-34
DEPDC5	0.509307831	1.74E-34
SLC25A23	0.508819573	2.06E-34
WNK3	0.508777021	2.09E-34
STAG3	0.508481836	2.31E-34
CCNE2	0.508206218	2.54E-34
TCP11	0.506430445	4.67E-34
MT2P1	-0.504948394	7.75E-34
AL021391.1	0.504914039	7.85E-34
AL359979.2	0.504502497	9.03E-34
TMTC2	0.504117967	1.03E-33
GRHL2	0.50262428	1.71E-33
AC002350.2	0.502284229	1.91E-33
FAM222A	0.50226288	1.93E-33
PLEKHA7	0.501637165	2.38E-33
TCHP	0.501623387	2.39E-33
PGBD2	0.500810044	3.15E-33
ZNF879	0.500779325	3.18E-33
PPP1R3D	0.499738374	4.51E-33
SUSD4	0.498919925	5.93E-33
RBMXL1	0.498607002	6.58E-33
SH2D4A	0.49789095	8.36E-33
AFTPH	0.497155131	1.07E-32
TMPRSS2	0.496657313	1.26E-32
CEP70	0.496353869	1.39E-32
STOX2	0.496027602	1.55E-32
USP54	0.495725253	1.71E-32
ERBB3	0.495609298	1.78E-32
TMEM168	0.495397081	1.91E-32
GMCL1	0.494978133	2.19E-32
EHF	0.49466914	2.43E-32
MYO3A	0.494632375	2.46E-32
ITSN2	0.494588873	2.49E-32
KDM2B	0.493920406	3.11E-32
DIPK2A	0.493860965	3.17E-32
ARHGEF26	0.493798539	3.24E-32
MFSD6	0.493747335	3.29E-32
PARD6B	0.493727198	3.31E-32
MBTD1	0.493623559	3.43E-32
TIFA	0.49317222	3.97E-32
DYRK1A	0.491508301	6.85E-32
TLR5	0.491258583	7.43E-32
PBX1	0.490839099	8.51E-32

Table S2. Functional analysis of the top 100 genes most closely related to lncRNA EP300-AS1

ONTOLOGY	ID	Description	GeneRatio	BgRatio	*p* value	p.adjust	qvalue
BP	GO:0072331	Signal transduction by p53 class mediator	8/80	267/18670	1.88e-05	0.022	0.021
BP	GO:0006260	DNA replication	7/80	274/18670	1.73e-04	0.069	0.067
BP	GO:0006282	Regulation of DNA repair	5/80	122/18670	1.78e-04	0.069	0.067
BP	GO:2001020	Regulation of response to DNA damage stimulus	6/80	214/18670	3.14e-04	0.091	0.088
CC	GO:0031519	PcG protein complex	3/80	47/19717	9.17e-04	0.091	0.079
CC	GO:0070160	Tight junction	4/80	128/19717	0.002	0.091	0.079
CC	GO:0035098	ESC/E(Z) complex	2/80	16/19717	0.002	0.091	0.079
CC	GO:0035267	NuA4 histone acetyltransferase complex	2/80	20/19717	0.003	0.091	0.079
CC	GO:0043189	H4/H2A histone acetyltransferase complex	2/80	20/19717	0.003	0.091	0.079
KEGG	hsa04218	Cellular senescence	6/35	156/8076	4.82e-05	0.005	0.004
KEGG	hsa03460	Fanconi anemia pathway	4/35	54/8076	8.02e-05	0.005	0.004
KEGG	hsa05223	Non-small cell lung cancer	4/35	72/8076	2.47e-04	0.010	0.009
KEGG	hsa05215	Prostate cancer	4/35	97/8076	7.70e-04	0.024	0.021

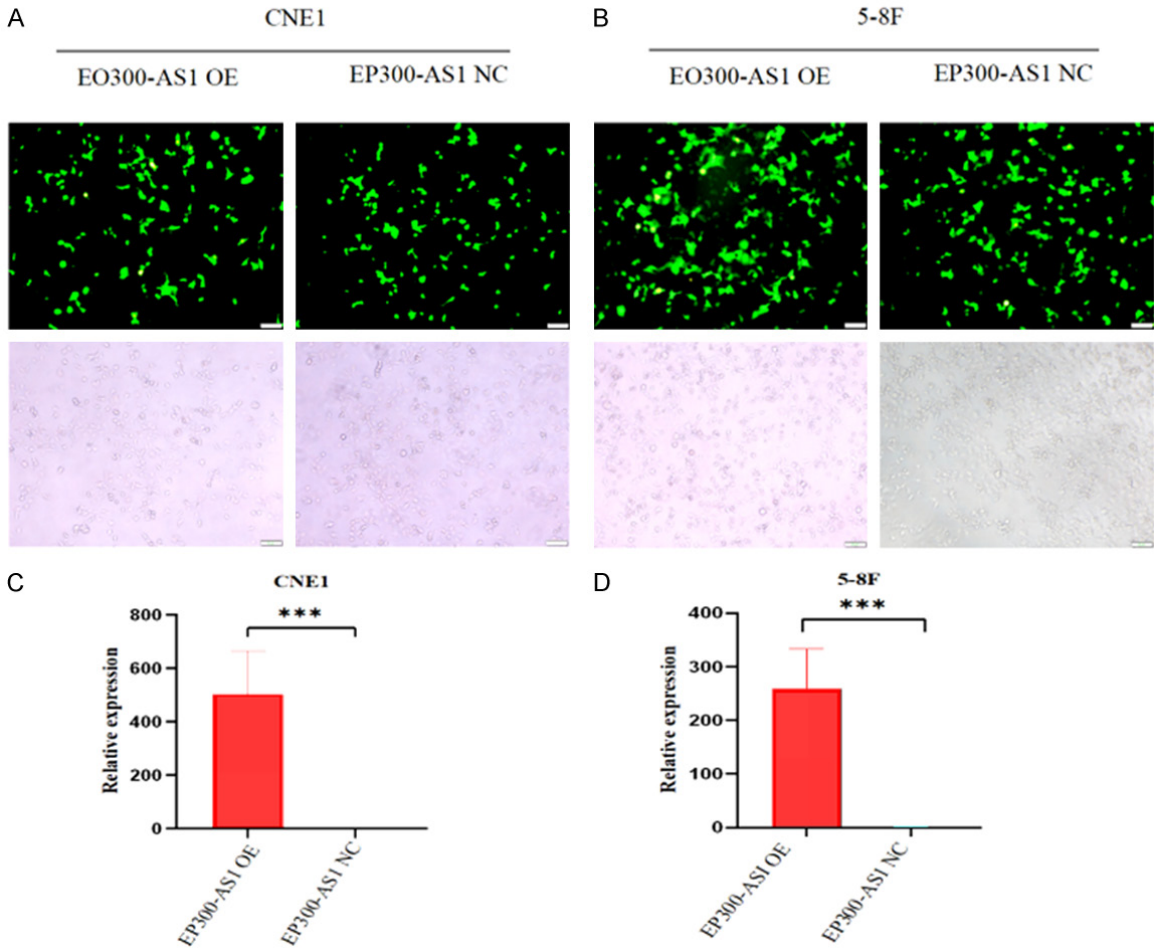

Figure S1. Transfection efficiency and detection of lncRNA EP300-AS1 plasmid. A, B. GFP-based visualization of transfection efficiency following overexpression of lncRNA EP300-AS1 in CNE1 and 5-8F cell lines. C, D. Verification of lncRNA EP300-AS1 overexpression using RT-PCR in CNE1 and 5-8F cell lines.

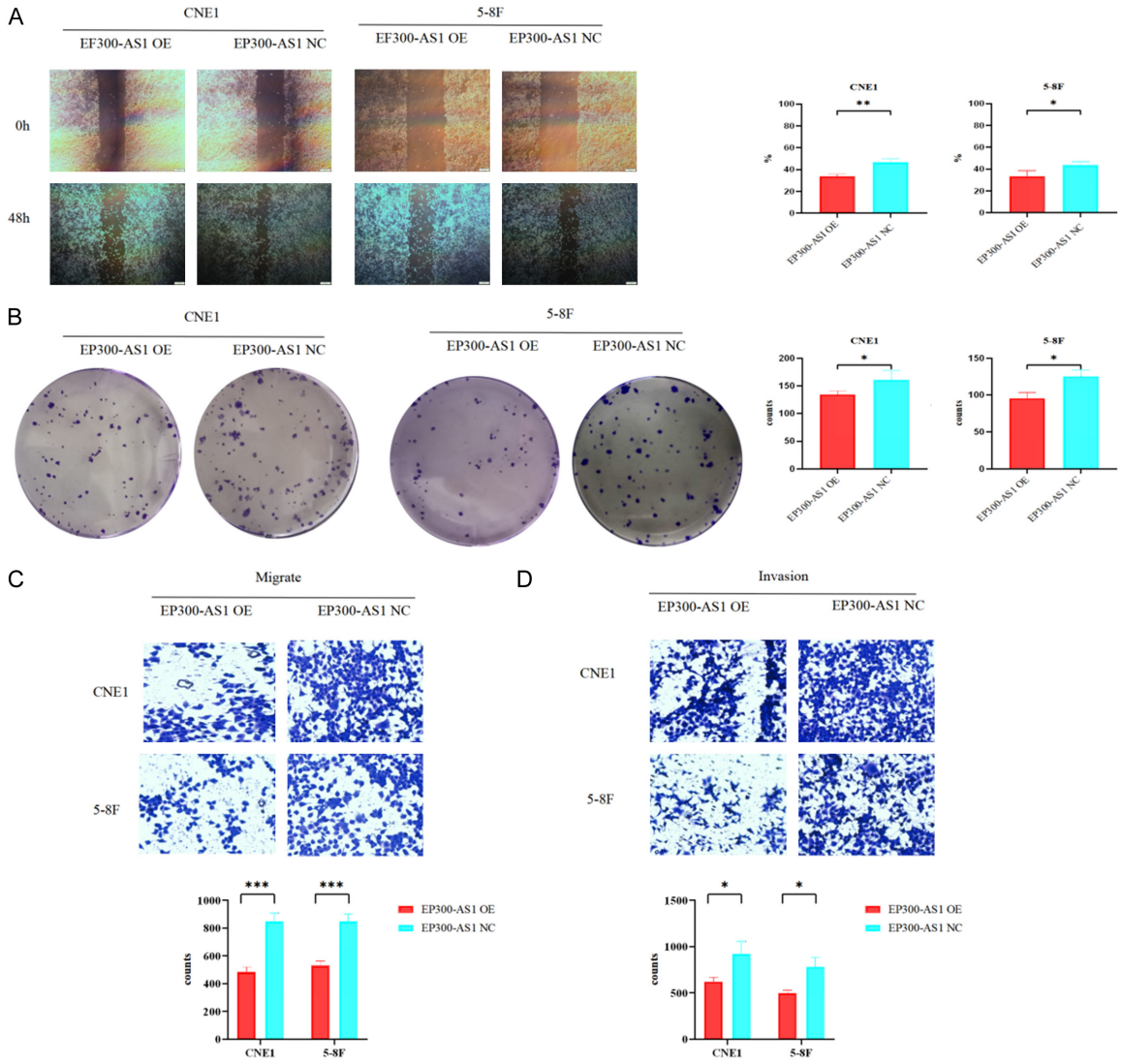

Figure S2. Effect of overexpressed lncRNA EP300-AS1 on NPC migration, invasion, and colony formation. A. Wound healing assays were conducted to measure the cell migration capacity. B. Colony formation experiments were carried out to detect cell cloning capacity. C. Transwell invasion tests were used to assess the migration of normal NPC cells and lncRNA EP300-AS1 overexpressed cells. D. Transwell invasion tests were used to assess the invasion of normal NPC cells and lncRNA EP300-AS1 overexpressed cells.

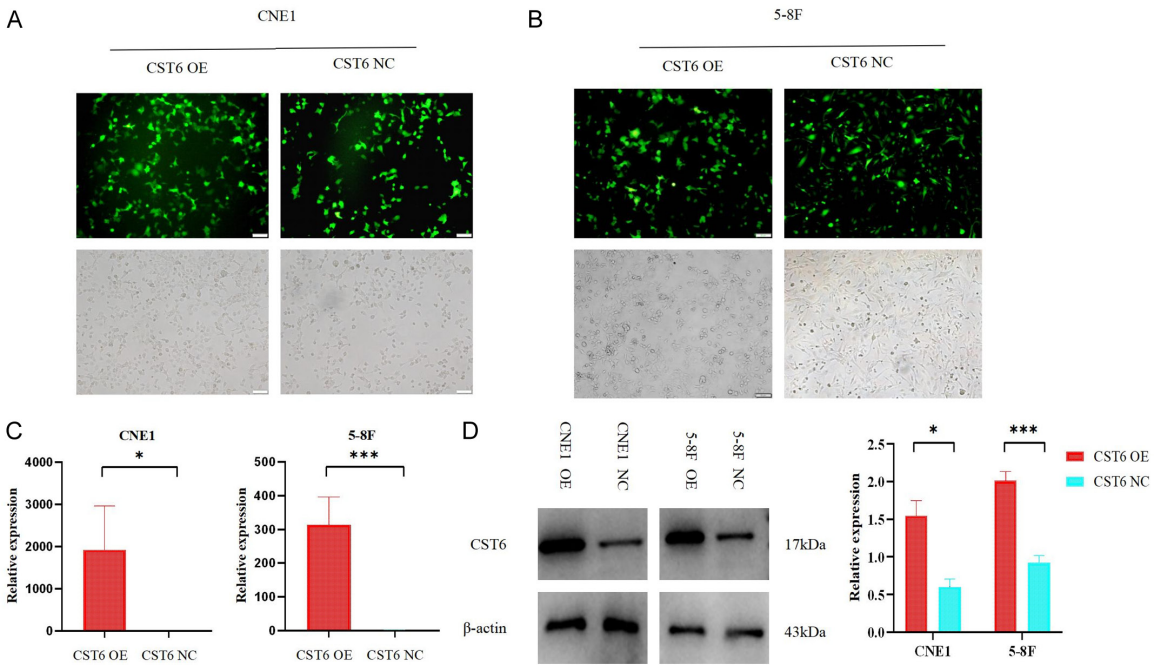

Figure S3. Transfection and detection of CST6 plasmid. A, B. Transfection efficiency was assessed using GFP after overexpression of CST6 in CNE1 and 5-8F cells. C, D. Transfection efficiency was measured using RT-PCR after overexpression of CST6 in CNE1 and 5-8F cells.

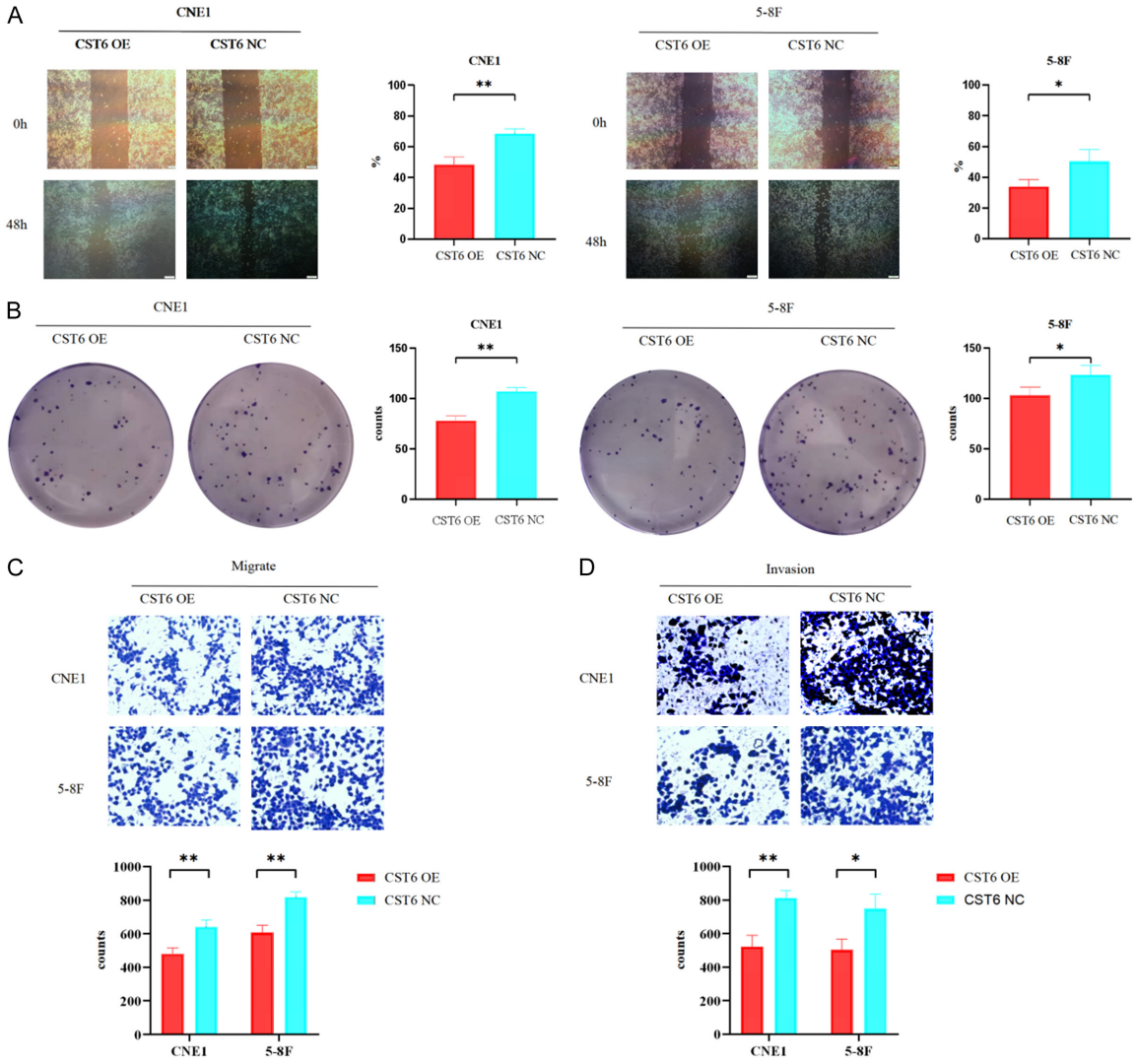

Figure S4. Effect of overexpressed CST6 on NPC migration, invasion, and colony formation. A. Wound healing assays were conducted to measure the capacity for cell migration. B. Colony formation experiments were carried out to detect cell cloning capacity. C. Transwell invasion tests were used to assess the migration of normal NPC cells and CST6-overexpressed cells. D. Transwell invasion tests were used to assess the invasion of normal NPC cells and CST6-overexpressed cells.